NASA Technical Memorandum 85966

NASA-TM-85966 19840024681

Superfluid Helium II Liquid-Vapor Phase Separation: Technology Assessment

Jeffery M. Lee

July 1984

National Aeronautics and Space Administration

NASA Technical Memorandum 85966

Superfluid Helium II Liquid-Vapor Phase Separation: Technology Assessment

Jeffery M. Lee, Ames Research Center, Moffett Field, California

National Aeronautics and
Space Administration

Ames Research Center
Moffett Field, California 94035

This Page Intentionally Left Blank

SYMBOLS

A	porous-plug flow area
A_{GM}	Gorter-Mellink parameter
APS	active phase-separator
A_p	total pore area available for flow
A_T	flow cross-sectional area of porous plug
C	specific heat capacity
COBE	Cosmic Background Explorer
d	channel diameter, active phase-separator gap width
d_g	flow-channel diameter
d_p	pore diameter
F	porous-plug geometry factor
GIRL	German Infrared Telescope Facility
g	gravitational constant
h	liquid level height above porous plug
IRAS	Infrared Astronomy Satellite
IRT	infrared telescope
j	mass-flux density, $g/sec \cdot cm^2$
K_{app}	apparent thermal conductivity
K_p	permeability, cm^2
K_{pn}	normal fluid permeability
ℓ	porous-plug thickness, active phase-separator gap length
MSFC	Marshall Space Flight Center
$\dot{m}$	mass flow rate, mg/sec
N_g	number of grains
N_p	number of pores
N_q	dimensionless heat flux

N_{Re}	dimensionless heat-flow Reynolds number
$N_{Re(c)}$	critical heat-flow Reynolds number
$N_{\nabla T}$	dimensionless thermal driving potential
P	pressure
ΔP	pressure difference
∇P	pressure gradient
Q	heat, J
$\dot{Q}$	heat-flow rate, W
q	heat-flux density, W/cm^2
R	APS radius of annular gap
S	entropy
SFHE	Superfluid Helium Experiment
SIRTF	Space Infrared Telescope Facility
T	temperature
T_{room}	room temperature
t	time
V	volume
$\dot{V}$	volumetric flow rate
v	velocity
v_c	critical velocity, laminar-to-turbulent flow
Z	APS geometry factor = $(2\pi/12)Rd^3/\ell$
ε	porosity
η	viscosity, g/cm·sec
λ	latent heat
ρ	density
σ	surface tension

Subscripts:

b	bath
c	critical condition, laminar-to-turbulent flow
d	downstream
ext	external
max	maximum value
n	normal fluid
p	pore size
s	superfluid
T	thermomechanical

SUMMARY

A literature survey of helium-II liquid-vapor phase separation is presented. Currently, two types of He-II phase separators are being investigated: porous, sintered metal plugs and the active phase-separator. The permeability K_p shows consistency in porous-plug geometric characterization. Passive phase-separation using porous plugs has been demonstrated for heat fluxes ranging from 1.0 mW/cm^2 to 100 mW/cm^2, with corresponding mass fluxes of from 0.1 $mg/sec \cdot cm^2$ to 10 $mg/sec \cdot cm^2$, respectively. These results cover a K_p range of 10^{-11} cm^2 to 10^{-9} cm^2. Both the heat and mass fluxes increase with K_p. Downstream pressure regulation to adjust for varying heat loads and bath temperatures is possible. For large dynamic heat loads, the active phase-separator has shown a maximum heat-rejection rate of up to 2 W and bath temperature stability of 0.1 mK. This report recommends that porous-plug phase-separation performance be investigated for application to SIRTF and, in particular, that plugs of 10^{-9} $cm^2 < K_p < 10^{-8}$ cm^2 in conjunction with downstream pressure regulation be studied.

1. INTRODUCTION

There will be a number of difficult problems associated with the performance of future infrared space telescopes in the space environment. One crucial requirement is that of maintaining the IR detectors at temperatures less than 2 K while rejecting sizable heat loads, and in so doing, maximizing lifetimes. Current cyrogenic technology utilizes the latent heat of liquid helium II for cooling. In such systems, a porous plug may be used to define the position of the liquid-vapor interface in near zero-g fields. The feasibility of these approaches has been proved by the successful operation of the Infrared Astronomy Satellite (IRAS) (ref. 1), where heat loads and temperatures remained relatively constant. Similar programs have since followed the same path, for example, the Cosmic Background Explorer (COBE) and the Infrared Telescope (IRT). The operation of future space missions, however, will impose more demanding requirements. In particular, the Space Infrared Telescope Facility (SIRTF) may require that variable heat loads ranging over a tenfold span be rejected, while IR detectors be maintained at 1.8 K and have operational lives of more than 2 yr. Therefore, there is a need to determine the limits of He-II phase separation as applied to SIRTF and other appropriate projects.

Four U.S. groups have done recent investigations on porous-plug phase separation. In addition, a German group has studied both porous plugs and the active phase-separator (APS). Explanation and prediction of the performance of He-II phase separation has led to diverse and nonconciliatory efforts between the various investigating groups. In short, each group proposes different explanations of the available experimental data. Summarizing these abundant data in a single, comprehensive report is no simple task, because the variations between experimental systems and procedures are so wide ranging. Still, an attempt is made here to present the available knowledge as a survey-type report that will provide future investigators with a quick and easy-to-use reference to the current published data and to the viewpoints

of the various groups. In addition, areas recommended for further study are included. These recommendations will be directed toward the application of porous-plug phase separation to SIRTF.

The report is divided into four sections. Section 1 reviews He-II hydrodynamics based on the two-fluid model and also presents theories relating the two-fluid model to phase separation. Sections 2 and 3 describe porous-plug and APS experimental systems and performance, respectively, and section 4 presents conclusions and recommendations.

2. THEORY

Two-Fluid Model

Liquid helium exhibits peculiar properties under certain conditions. It is these properties, among others, that qualify it for use as a cooling agent for IR detectors at temperatures below 2 K in a zero-g environment.

Figure 1 shows the phase diagram of helium. There are two liquid phases of helium: He I and He II. He I obeys the laws of classical Newtonian mechanics; He II has the properties of superfluidity. The phase transition between He I and He II is referred to as a lambda transition and is characterized by the increase in the heat capacity to an infinite value at the temperature (T_λ) and pressure (P_λ) of the phase change, that is, the lambda point (inset of fig. 1).

A peculiar property of He II is that a temperature gradient produces a pressure gradient. Figure 2 shows this experimentally. The name given to this phenomenon is the fountain effect, or the thermomechanical effect. It is exactly this phenomenon, together with an appropriate porous-plug geometry, that is used to contain the liquid in a zero-g environment for liquid-vapor phase separation.

The model used to describe the mechanism of transport in He II has been termed the two-fluid model; it was independently proposed by both Tisza (ref. 2) and Landau (ref. 3). According to the two-fluid model, He II can be thought of as being composed of two separately interacting fluid components: a normal fluid component having finite viscosity and entropy and a superfluid component having zero viscosity and zero entropy. The combination of the two components thus gives rise to the bulk liquid properties,

$$\rho = \rho_s + \rho_n \tag{1}$$

where ρ is the bulk-fluid density and $\rho_s/\rho \to 1$ as $T \to 0$ K and $\rho_n/\rho \to 1$ as $T \to T_\lambda$. Both the superfluid and normal fluid density ratios are functions of temperature. Figure 3 shows this experimentally measured relationship. The total laminar-flow description of He II, then, is described in terms of the independent equations of motion for the normal and superfluid (refs. 4-6):

$$\rho_n d\vec{v}_n/dt = -(\rho_n/\rho)\nabla P - \rho_s S\nabla T + \rho_n \nabla^2 \vec{v}_n \tag{2}$$

$$\rho_s d\vec{v}_s/dt = -(\rho_s/\rho)\nabla P + \rho_s S\nabla T \tag{3}$$

From equation (3) for the superfluid component under steady-state conditions and laminar transport, the fountain effect is described according to

$$\nabla P_T = \rho S \nabla T \tag{4}$$

The bulk mass-flux density $\vec{j}$ is just the vector sum of the two components

$$\rho v = \rho_n \vec{v}_n + \rho_s \vec{v}_s \tag{5}$$

$$= \vec{j} = \vec{j}_n + \vec{j}_s \tag{6}$$

Two major regions of heat transport are observed: laminar linear transport where $q \propto \Delta T$, and nonlinear turbulent transport with $q \propto (\Delta T)^{1/3}$. To describe the laminar heat flow, the thermal energy content is carried by the normal fluid component (ref. 7):

$$\bar{q} = (\rho S T) v_n \tag{7}$$

Under conditions of zero net mass flow, where $j = 0$ and $\rho_n v_n = -\rho_s v_s$, the normal and superfluid components flow in opposite directions with respect to each other. That is, the normal fluid flows down the temperature gradient as a classical Newtonian fluid, while the superfluid flows up the temperature gradient producing the fountain pressure. Thus, transport is seen to be convective rather than conductive. Experimental measurements of the apparent thermal conductivity ($K_{app} = -q/\nabla T$) shows a heat flux that can be up to 800 times greater than that of copper.

For fully developed turbulent transport, commonly known as Gorter-Mellink (GM) turbulence (ref. 8), a mutual friction between the two components gives rise to the nonlinear heat-flux relation,

$$q = \rho_s S T (S |\nabla T| / \rho_n A_{GM})^{1/3} \tag{8}$$

where A_{GM} is the Gorter-Mellink parameter and is a function of pressure and temperature. Note that the GM region is independent of the flow duct diameter. Investigation of this transport has been extensive (refs. 8-12).

Attempts to predict the critical transition between laminar and turbulent flow have incorporated the use of a dimensionless heat-flow Reynolds number (N_{Re}). Dimotakis (ref. 13) has proposed that for zero net mass flow, $N_{Re} = (q \ell A_{GM}/ST)$ where ℓ is the geometric characteristic length. The critical transition has been found to be $N_{Re(c)} = 1$ for long, insulated cylindrical channels where $\ell = \pi d$.

Phase Separation

Numerous studies of He-II heat transport have been conducted under zero net mass-flow conditions (fig. 2). However, for phase separation, vapor is on one side of a thermo-osmotic filter (the phase separator) and liquid is on the other side.

Figure 4 shows the general conditions required for satisfactory phase separation in a terrestrial environment. Under saturated vapor conditions, the downstream temperature T_d is less than the bath temperature T_b. Both T_d and T_b are less than the lambda temperature. This creates the necessary temperature gradient across the phase separator to produce the fountain pressure, ΔP_T. It is the fountain pressure

that will contain the liquid helium within the Dewar. The liquid will stay confined only if ΔP_T is greater than the sum of the applied and static pressure heads.

Currently, two types of phase-separation devices are being explored: the active phase-separator (APS) and sintered porous metal plugs. The theoretical flow description through both devices uses the two-fluid model equations that are referenced with respect to zero net mass-flow conditions. Phenomenological descriptions have also been published. In general, certain assumptions and corresponding equations are seen repeatedly throughout the literature; they are presented below.

1. A heat balance around the phase separator, assuming saturated vapor conditions, requires that the heat rejected through the separator be proportional to the mass-flow rate. The proportionality constant is the latent heat of vaporization, λ:

$$\dot{Q} = \dot{m}\lambda \tag{9a}$$

The heat-flux density is thus

$$q = \dot{m}\lambda/A = j\lambda = \rho v\lambda \tag{9b}$$

2. The normal fluid assumes laminar Newtonian mechanics:

$$\nabla P = \eta_n \nabla^2 v_n \tag{10}$$

the normal fluid viscosity being η_n.

3. The steady-state equations of the two-fluid model are applicable to steady-state phase separation.

4. (Specific to porous-plug phase separators.) The flow is assumed to be laminar Darcy flow with the permeability K_p a characteristic of the porous media flow geometry:

$$\dot{V}/A_T = K_p \nabla P/\eta \tag{11}$$

where A_T is the superficial cross-sectional area of the plug, $\dot{V}$ is the volumetric flow rate, and η is the fluid dynamic viscosity.

Active phase-separator- Theoretical transport in the APS has been studied by Schotte. In brief, the APS utilizes an annular gap to obtain phase separation. A more detailed description of APS design and operation is given in section 3.

Schotte (refs. 14 and 15) and Schotte and Denner (ref. 16) have presented a theoretical model for He-II transport. In a moving coordinate system with velocity v, equation (7) becomes

$$q = \rho ST(v_n - v) \tag{12}$$

Combining this with equation (9b) yields

$$\rho v\lambda = \rho ST(v_n - v) \tag{13}$$

which may be solved for ρv:

$$\rho v = \rho S T v_n / (ST + \lambda) \tag{14}$$

The normal fluid assumes flow according to the Hagen-Poiseuille equation,

$$v_n = (d^2/12\eta_n)\nabla P \tag{15}$$

Substitution of ρv for the measurable superficial quantities $\dot{m}/A$ and of equation (15) into equation (14) yields the total mass flow through the phase separator,

$$\dot{m} = Z(\rho/\eta_n)[ST/(ST + \lambda)]\Delta P \tag{16}$$

where the geometry factor is $Z = (2\pi/12)Rd^3/\ell$ for an annular gap; R is the radius of the annular gap; and d is the channel width. Equation (16) reduces to

$$\dot{m} = Z\rho/\eta_n(ST/\lambda)\Delta P \tag{17}$$

at low T where $\lambda >> ST$. Equation (17) can also be obtained for a stationary coordinate system ($v = 0$).

Porous-plug phase separators- A number of groups have studied phase separation through porous plugs. The principal investigators of the various groups are

1. M. DiPirro, currently associated with COBE

2. T. H. K. Frederking et al., UCLA Cryogenic Engineering Laboratory

3. J. Hendricks et al., associated with IRT

4. D. Petrac and P. V. Mason, associated with IRAS and the Superfluid Helium Experiment (SFHE)

In addition, studies have also been conducted by

5. M. Murakami et al., Institute of Structural Engineering, University of Tsukaba, Japan

6. H. D. Denner, G. Klipping et al., Fritz-Haber Institut der Max-Plank-Gesellschaft, Berlin, and U. Schotte, Institut für Theoretische Physik, Freie Universität, Berlin, associated with the German Infrared Laboratory (GIRL)

7. G. R. Karr and E. W. Urban, Marshall Space Flight Center (MSFC), IRT project

Following is a brief description of the theoretical and phenomenological equations used by the various investigators in their studies of porous-plug phase separators. Where appropriate, equations are compared between groups.

Hendricks and Karr (refs. 17 and 18) have proposed flow models based on a number of possible flow geometries. Poiseuille flow in straight channels of diameter d is assumed, with d determined in different ways. Schotte's flow description (eq. (16)) is used with basic variations to the Z factor. Using

$$Z = (A_p/\ell)(d_p^2/32) \tag{18}$$

where A_p is the total pore area available for flow, three cases have been presented:

1. $A_p = \varepsilon A_T$, where ε is the plug porosity

2. $A_p = N_g d_g^2$, where N_g is the number of grains and d_g is the flow channel diameter

3. $A_p = N_p \pi d_p^2/4$, where N_p is the number of pores and d_p is the pore diameter based on the filtration test

Evaluations have been conducted to determine the validity of these models based on the prediction of the laminar-to-turbulent transition region (ref. 18). Results obtained indicate that the geometry of item (2) above best describes the geometry of porous plugs, but larger by a factor of 10 than that predicted under zero net mass-flow conditions (ref. 18). Opinions about the mechanism of the transition to turbulent flow seem to be of current interest. Many investigators (ref. 19; P. V. Mason 1984: personal communication; J. B. Hendricks 1984: personal communication; and M. DiPirro 1984: personal communitation) believe that the liquid-vapor interface retreats within the pores of the plug during turbulent flow. The mechanism of transport is controversial, however.

DiPirro et al. (ref. 19) and DiPirro (ref. 20) have considered the effects of the surface tension in determining the position of the interface with respect to the plug. A force balance over the interfacial surface under saturated vapor conditions results in

$$\rho S \Delta T - (dP/dT)\Delta T - \rho g h = \sigma(dA/dV) \tag{19}$$

where $\sigma(dA/dV)$ is the surface free-energy per unit area. For conditions in which the fountain effect becomes large, the interface is thought to retreat within the plug until equation (19) is satisfied. Equation (19) predicts the point at which a steep rise in ΔT should be observed for increasing T_b. Data, as obtained by DiPirro et al. (ref. 19), show the transition to be within reason, as predicted by equation (19).

Karr and Urban (ref. 21) have proposed the description of He-II heat transfer in the form of Fourier's law,

$$q = -K_{app} \nabla T \tag{20}$$

The apparent thermal conductivity K_{app} is assumed to be dominated by the conductivity of the liquid. Taking the apparent thermal conductivity of the liquid (ref. 22) to be $K_{app} = \rho^2 S^2 T d^2/12\eta_n$, and A_T scaled by the porosity, ε, gives the mass flux through a porous plug,

$$\dot{m}/A_T = \rho(d^2/12)\varepsilon(\Delta P/\eta_n)(ST/\lambda) \tag{21}$$

For predicting the laminar-to-turbulent transition, the effort of Dimotakis (ref. 13) is used. Under conditions where the superfluid velocity is less than a critical value, v_c, laminar flow is predicted by equation (22):

$$v_s/v_c \leq d^3/\ell(\pi\varepsilon\Delta P S T A_{GM}/12\eta_n\lambda) \tag{22}$$

Yuan (ref. 23), Yuan and Frederking (ref. 24), and Lee et al. (ref. 25) have proposed normal fluid Darcy flow as a solution to the steady-state force balance between the normal and superfluid. Addition of equations (2) and (3), neglecting inertial effects, yields

$$\nabla P = \eta_n \nabla^2 v_n \tag{23}$$

which is just a Newtonian description of the normal fluid, equation (10). A solution to equation (23) can be written in the form of normal-fluid Darcy transport subject to Newtonian boundary conditions:

$$v_n = K_{pn} \nabla P_T / \eta_n \tag{24}$$

It is noted that in equation (24), $\nabla P = \nabla P_T$ (eq. (4)) and K_{pn} is the normal-fluid permeability analogous to K_p of equation (11).

The nondimensional form of equation (24) is written as

$$N_q = N_{\nabla T} \tag{25}$$

with

$$\left.\begin{aligned} N_q &= \bar{q} K_{pn}^{1/2} / \eta_n S T \\ N_{\nabla T} &= \rho^2 S |\nabla T| K_{pn}^{3/2} / \eta_n^2 \end{aligned}\right\} \tag{26}$$

where N_q is a normalized heat-flow Reynolds number, and $N_{\nabla T}$ is the thermal driving force (refs. 24 and 26). Equation (23) applies to zero net mass-flow conditions. Geometric characterization of a porous plug at liquid helium temperatures has been found to be useful, using K_{pn} as the characteristic dimension. For phase separation with superfluid/normal counterflow, equations (6), (7), and (9b) combine to give

$$|v_s| = (\rho_n/\rho - ST/\lambda)\bar{q}/(\rho_s ST) \tag{27}$$

At low temperature, where $\rho_n/\rho << ST/\lambda$, an asymptotic approach to zero net mass flow is predicted (refs. 25 and 27) and equation (25) applies. Figure 5 shows this approach to $j = 0$ for various porous media tested under phase-separation conditions (T. H. K. Frederking 1984: personal communication).

For fully developed Gorter-Mellink convection in a long, insulated channel where the channel diameter d is the characteristic length (ref. 30),

$$N_q \rho / \rho_s = K_{GM} (N_{\nabla T} \rho_s / \rho_n)^{1/3} \tag{28}$$

Note that equation (27) is independent of d. Evaluation of data for zero net mass flow with $N_{\nabla T} \rho_s / \rho_n$ ranging over 10 orders of magnitude shows $K_{GM} = 11.3 \pm 1.4$ (K_{GM} is the universal Gorter-Mellink constant). For smaller ducts with diameters of the order of 0.1 to 10 μm, as encountered with porous plugs, K_{pn} shows possible duct diameter dependence (ref. 27). These smaller ducts correspond to permeabilities of the order of 10^{-9} cm^2 to 10^{-8} cm^2. Equation (27) has been applied with relative success to quasi-steady phase separation (refs. 27 and 31).

Petrac and Mason (ref. 32) have given a phenomenological description of phase separation based on experimental data. The mass flow through the plug is found to be proportional to the applied pressure gradient under laminar conditions, the proportionality constant being related to the plug geometry,

$$\dot{m} = (FA)\Delta P \tag{29}$$

where F is the plug geometry factor involving the "flow-channel size," fluid viscosity, and superficial plug thickness. Equation (29) is related to K_{pn} of the thermo-osmotic Darcy equation by

$$K_{pn} = (F/\rho ST)\ell\eta(\Delta P/\Delta P_T) \tag{30}$$

The F-factors of a variety of different porous media tested by Petrac and Mason are included in table 1.

3. POROUS-PLUG INVESTIGATIONS

Test Systems

The general system employed for studying He-II phase separation using porous plugs is depicted in figure 6. The porous plug is bonded at the end of a thermally insulated vent line which, in turn, is dipped into a He-II bath. The He-II bath represents the Dewar system. System parameters that are measured are the mass-flow rate through the plug, $\dot{m}$; the downstream and bath temperatures, T_d and T_b, respectively; the downstream and upstream bath vapor pressures, P_d and P_b, respectively; the liquid level above the plug, h; and the applied pressure difference across the plug, $\Delta P = P_b - P_d$ (downstream and upstream are referenced with respect to the finite mass flow of helium through the plug). Operational conditions for phase separation usually require $T_d < T_b < T_\lambda$ and $\Delta P + \rho gh < \Delta P_T$. However, under certain conditions, T_b may be greater than T_λ, provided that $T_d < T_\lambda$ (ref. 32). In this case, the lambda transition occurs within the plug. A heater in the bath may be used to simulate various heat loads on the Dewar system. Downstream vent-line impedance may or may not be adjustable.

Preferred plug materials are low-conductivity metals and ceramics. The plug may be inserted in the vent line using an indium O-ring seal and pressure coupling (refs. 17 and 19) or it can be bonded to the vent line by either epoxy adhesives or welding (ref. 27; J. B. Hendricks 1984: personal communication; M. DiPirro 1984: personal communication). Temperatures are measured by germanium or carbon resistance thermometers. Downstream and upstream pump filters and liquid N_2 cold traps are used to minimize plug contamination and to ensure accurate mass-flow readings. Vent-line radiation shields should be incorporated where appropriate.

When operating, heat absorbed by the bath will be rejected through the plug via the latent heat of the finite liquid mass flow. Ideally, the liquid-vapor interface occurs at the downstream surface of the plug, though it has been hypothesized that under certain conditions, the interface may retreat within the plug pores (ref. 19; J. B. Hendricks 1984: personal communication; M. DiPirro 1984; personal communication). Conditions may also result in liquid downstream of the plug (breakthrough conditions). Under ideal operation, laminar transport is realized. Consequently, there is minimal resistance to the heat flow and large $\dot{m}$'s are obtainable at smaller ΔP's. In this laminar region, $d\dot{m}/d\Delta P$ may be of the order of 10 mg/(sec·Torr) (ref. 17), but this is dependent on K_p. For turbulent flow,

$d\dot{m}/d\Delta P$ may be reduced by two orders of magnitude, hence operation in the turbulent region places severe constraints on the maximum amount of heat that can be rejected by pure phase separation for a given plug area. Between laminar and turbulent flow is the transition region where $d\dot{m}/d\Delta P$ decreases as ΔP increases; it can be characterized by a critical $\dot{m}_c$ and critical ΔP_c.

When designing a system to test the maximum $\dot{Q}$ capabilities of a plug, $\dot{Q}_{max}$, pressure-drop considerations will be important. The maximum ΔP across the plug is determined by the difference between the bath vapor pressure and the total downstream vent-line pressure drop. This, in turn, dictates the limits on $\dot{m}_{max}$ and $\dot{Q}_{max}$. To obtain higher $\dot{m}_{max}$ and $\dot{Q}_{max}$, either a greater ΔP must be achieved, or the plug resistance must be decreased. The first alternative can be obtained by reducing the pressure drop downstream in the vent line. The second alternative is possible by altering the plug geometry: pore size, area, and thickness. It is noted that the maximum ΔP's available will be characteristic of the pumping system employed (refs. 27 and 33).

Experimental parameters commonly recorded are $\dot{m}$, ΔP, T_d, T_b, P_d, and P_b. Since there is only one degree of freedom, the bath temperature T_b is often fixed, and data are taken under steady-state conditions (refs. 17 and 34; D. Petrac 1979: unpublished report). A typical set of data is exhibited in figure 7(a) (D. Petrac: unpublished report). To obtain a different T_b, a combination of heater input to the bath and of outer bath vapor pressure or downstream vapor pressure or both must be appropriately adjusted. In this manner, steady-state bath isotherms are obtained.

Some investigators have studied phase separation under quasi-steady-state conditions (refs. 21, 29, 31, and 33). A representative set of data is given in figure 7(b) (ref. 29). These results can be compared to constant bath temperature results only if dT_b/dt is kept small or if transient effects are accounted for. In the latter case, the mass-flow rate is then $\dot{m} = \rho VC\, dT/dt + \dot{Q}_{in}$, where C is the system heat capacity per unit mass, t is the time, and $\dot{Q}_{in}$ is the total heat input to the Dewar (applied plus parasitic). Dynamic response of a porous-plug system would be important, however, where transient Dewar heat loads or stored heat that needs to be rejected are of interest. Such would be the case when the vent line is opened after a launch to cool the system down to operating temperatures or when only a small amount of helium remains and the total system heat capacity cannot adequately maintain temperature stability.

Flow Control

Methods of flow control are of considerable interest. Many schemes of flow modulation have been proposed and investigated. In particular, flow control by use of a downstream pressure regulating device shows promise. This scheme has the advantage of simplicity of operation and of minimizing the number of cryogenic mechanical components.

The use of a downstream heating element to vary the temperature difference across the plug has also been studied (refs. 21 and 34). In this system, the control of the fountain pressure is used to regulate the mass-flow rate. Figure 8 shows the change in $\dot{m}$ as a function of ΔT across a 10-μm ceramic porous plug with $T_b = 1.90$ K and $\Delta\dot{m} = \dot{m} - \dot{m}\,(\dot{Q}_{ext} = 0)$; $\dot{Q}_{ext}$ is the applied heat flow downstream of the plug (ref. 34). A linear relation between $\dot{m}$ and ΔT is observed, as predicted by the two-fluid model (λ is not a strong function of temperature in this

range of T) with $\Delta\dot{m}$ inversely related to ΔT. The slope $(d\Delta\dot{m}/d\Delta T) = 4.2$ mg/(sec·K) with ΔT ranging from 0 to 1.5 K.

Figure 9 shows the transient response of the downstream pressure as a function of step inputs in $\dot{Q}_{ext}$ (ref. 21). The response has been written as a time-dependent exponential function, with

$$P_d(t) = P_1[1 - a_1 \exp(-b_1 t)] \tag{31}$$

for increased step inputs in $\dot{Q}_{ext}$ and with P_1 the final pressure as $t \to \infty$, a_1 the proportionality constant, and b_1 the time-constant. For decreased step inputs in $\dot{Q}_{ext}$,

$$P_d(t) = P_2[1 + a_2 \exp(-b_2 t)] \tag{32}$$

with P_2, a_2, and b_2 the final downstream pressure, proportionality constant, and decay time-constant, respectively. Table 2 shows the measured values for a 5-μm ceramic plug (ref. 21). No values for a_1 and a_2 are given.

Heating of the Dewar bath is also possible, with the design of the system skewed toward the maximum anticipated heat loads. An important disadvantage, however, is the wasteful boiling off of liquid at low heat inputs.

A rotatable shutter assembly has been designed and tested (refs. 26, 27, and 31). In this system, the effective area available for flow through a plug is varied using a rotatable shutter assembly located on the downstream side of the plug. The shutter is driven by a motor via a connecting shaft. This proof-of-principle experiment has shown effective flow modulation of up to 60% from a mean value of 16 mg/sec.

Other possibilities include a parallel plug arrangement in which each plug has its own vent line and value. If initially a number of valves are closed, then $\dot{m}$ can be increased by opening a value to a particular plug. The flow area would then be distinctly defined and the limiting restrictions to the maximum available ΔP could be reduced for laminar flow operation. However, liquid breakthrough may occur in the closed vent lines if a sufficient ΔT is not present, and thermo-acoustic oscillations may increase heat leaks. Backstream pressure regulation of this parallel plug-valve arrangement is also possible.

Experimental Results

Though a number of groups have investigated porous-plug phase separation of He II and though a large amount of information exists, there seems to be a wide discrepancy in the explanation of the experimental results. This section will not necessarily attempt to explain the abundance of data with respect to the various proposed theories. Instead, the available experimental data will be presented under a common frame of reference, when possible, in an effort to provide a systematic presentation of porous-plug phase-separation performance. Table 1 lists the various plugs and corresponding references to the literature.

Plug characterization- It is common to characterize plugs according to the manufacturer's stated nominal pore size or nominal filtration size; however, this type of characterization shows wide variation between manufacturers. Nonstandardized methods and procedures in determining these "nominal sizes" account for this confusion. In

particular, sizes may be determined by methods of particle filtration or retention, or by bubble pressure testing (refs. 36 and 37). Despite these inconsistencies, pore size is often used to distinguish plugs. This report will not characterize plugs by pore size, however. Instead, the permeability K_p, as defined by Darcy's law (eq. (11)) has shown a degree of consistency and thus will be used to characterize plugs. Still, pore size will be retained and referred to for reader convenience.

Figure 10 shows K_p as a function of manufacturer's stated nominal size at room temperature (ref. 27). Mott Metallurgical Company and Pacific Sintered Metals (PSM) both use the particle filtration method in characterizing their plugs. The particle-retention size measurement has been conducted by independent testing facilities. A good relationship is observed between K_p and the nominal size for plugs of a single manufacturer, but there is a wide discrepancy between plugs of different manufacturers. Porous plugs from Mott show K_p to be an order of magnitude larger than K_p of PSM plugs for a given nominal size greater than 20 μm. At nominal sizes of 1 μm, K_p of Mott plugs is about 3 times as large as K_p of PSM plugs. The collimated plug of Petrac and Mason (ref. 32), which is a collection of finely drawn stainless steel capillary tubes (750,000, each with a diameter of .4 μm) shows a close correlation to the porous plugs of PSM.

Figure 11 shows the experimentally measured relation between bubble-pressure pore size and particle removal size. No well-defined relation between these two parameters is apparent, although a relationship between particle removal size and pore size can be deduced.

It has been found that K_p decreases with decreasing temperature (ref. 23). At liquid-helium temperatures under phase separation, it may be advantageous to characterize the plug according to the asymptotic limit to zero net mass flow, using K_{pn} of the thermo-osmotic Darcy equation as described in equation (24). In addition, K_{pn} has been found to approach the room temperature value of K_p as the zero net mass-flow asymptote is reached. Figure 12 shows this relation under phase separation for plugs of reference 29 and T. H. K. Frederking (1984: personal communication).

Phase separation- For a given plug with a characteristic K_p, there is a unique steady-state relation between $\dot{m}$, ΔP, and T_b that will trace out a surface contour much like a three-dimensional T, P, and V phase diagram. Increasing K_p will result in a higher surface, with the possibility of extended transport in the laminar regime, all else being constant. From this steady-state diagram, one can project a plane onto a two-dimensional graph with either $\dot{m}$, ΔP, or T_b as a constant parameter.

A common way of showing data is on a graph of $\dot{m}$ versus ΔP for various constant T_b's. Figures 7(a) and 13 show this interdependence for the results of two studies (ref. 17; and D. Petrac 1979: unpublished report). Apparent is a large initial slope $(d\dot{m}/d\Delta P)$, corresponding to ideal laminar flow. With an increase in ΔP, the slope $(d\dot{m}/d\Delta P)$ is drastically reduced. The point at which this transition from laminar to turbulent transport takes place is typically designated as $\dot{m}_c$ and P_c. It may be noted, however, that $\dot{m}_c$ and P_c characterize a region of transition rather than a distinct point. In addition, $\dot{m}_c$ and P_c increase with increasing T_b. Thus, two distinct flow regimes have been identified, with the transition from laminar to turbulent transport occurring within some intermediate region.

Laminar flow: Referring to figures 7(a) and 13, it can be seen that there is a severe restriction when operating porous-plug phase separation in the laminar-flow regime. That is, the transition to turbulence is encountered at very small ΔP's,

in the range of 0.24 to 1.5 Torr, depending on T_b and plug K_p. Figure 13 shows data for a 0.5-μm plug (ref. 17). Figure 7(a) shows terrestrial data for a 0.5-μm ($K_p = 10^{-9}$-cm^2) plug that is currently flying in IRAS (D. Petrac 1979: unpublished report).

Figure 14 shows the $\dot{m}$ versus ΔP relation for various T_b for larger pore size and permeability plugs. Larger K_p and larger A_T plugs can lead to an increase in $\dot{m}$ at substantially reduced values of ΔP. However, the information that has been compiled is not considered adequate to support definite conclusions. In particular, the data may not necessarily have been obtained under steady-state conditions at constant T_b. Transient heating owing to the system heat capacity may account for higher than expected $\dot{m}$'s with respect to steady-state T_b's. Further, the question of whether phase separation still exists or whether liquid breakthrough occurs at reduced ΔT's or large ΔP's is unanswered.

Figure 15 shows a graph in which the superficial plug geometry is eliminated as a factor in system performance. The coordinates are plotted as mass-flux density ($\dot{m}/A_T$) versus $\nabla P = \Delta P/\ell$. The effect of decreasing K_p results in a decrease in $\dot{m}/A_T$ for a given ∇P, as one would expect. This inverse relation between $\dot{m}/A_T$ and K_p suggests a Darcy-type approach in describing the superficial fluid flow. From an analysis such as this, the plug geometric parameters may be separated from the inherent fluid properties. If this is the case, then specification of a plug for a particular application can be done with thought to breakthrough conditions. For example, if a large amount of heat must be rejected and if the specifications for ΔP or ΔT across the plug create a liquid breakthrough condition, then a large-area plug of small K_p may be used. This, of course, depends on the ability to predict breakthrough conditions with respect to plug geometric parameters. Currently, there is a need to investigate breakthrough conditions in more detail.

Transition region: The mechanism of the transition from laminar to turbulent flow for phase separation is currently a matter of uncertainty. Some investigators suggest superfluid critical velocities initiating Gorter-Mellink turbulence. Others propose the retraction of the liquid-vapor interface within the plug that results in transport through a high resistance vapor phase. Still others suggest a combination of the two. The prediction of the transition region is still under investigation. The actual determination must be made for each individual plug under testing conditions.

Figure 16(a) presents results of the transition point of a 0.5-μm plug (ref. 17) as a function of T_b. The critical mass-flow rate $\dot{m}_c$ is seen to increase from 1.7 mg/sec to 5.7 mg/sec with increasing T_b from $T_b = 1.65$ K to 2.1 K. After $T_b = 2.1$ K, $\dot{m}_c$ decreases to 4.8 mg/sec at $T_b = 2.15$ K. The decrease may be due to the high superfluid velocity initiating turbulence at this lower value of $\dot{m}_c$ as $T_b \rightarrow T_\lambda$.

Turbulent transport: It is possible to operate a porous plug in the turbulent regime. An immediate consequence and restriction, however, is the quick approach to the maximum available ΔP as a result of the small values of $d\dot{m}/d\Delta P$. Figures 16(b) and 16(c) show $d\dot{m}/d\Delta P$ versus T_b for both the laminar and turbulent flow regimes, respectively, of a 0.5-μm plug (ref. 17).

From figure 16(b), $d\dot{m}/d\Delta P$ for laminar flow ranges from 9 mg/(sec·Torr) at $T_b = 1.65$ K to 28 mg/(sec·Torr) at $T_b = 2.1$ K. This is about 2 to 4 times greater than $d\dot{m}/d\Delta P$ for turbulent flow at the same bath temperatures. This stronger $\dot{m}$ dependence on ΔP and T_b for laminar flow can give wider ranges of control for a

given phase-separation system. But it may be more difficult to stabilize T_b and $\dot{m}$ in the laminar-flow region as opposed to the turbulent-flow region because of the greater dependence of $\dot{m}$ on ΔP. For plugs with larger K_p, it is possible that laminar transport may be extended to higher $\dot{m}_c$'s and ΔP_c's with respect to plugs with smaller K_p. However, there is insufficient information about this effect.

4. THE ACTIVE PHASE-SEPARATOR

System Description

The active phase-separator (APS) (refs. 38-40) is a dynamic device used to regulate mass flow. Regulation of $\dot{m}$ compensates for varying heat loads and changing bath temperatures.

Figure 17 shows a schematic of the APS. The APS, which is composed of a sliding pin situated within a bushing, is located at the exit vent line from the He-II Dewar. The defining geometry for fluid transport is thus an annular gap geometry of variable length. Tests have been conducted (ref. 38) using a parallel gap of 5 μm, a conical section with a gap variability of 5 to 15 μm, and an open circular groove. The diameter of the annulus is 20 mm, and the gap length ℓ varies from 0 to 15 mm. Under laminar flow conditions (with $\dot{m} < 7$ mg/sec), section AB of the pin is in the bushing. Phase separation thus occurs within section AB. For increased mass-flow requirements, the pin is extended out of the bushing to where point T (top of bushing) is within the limits of section BC of the moving pin. Here, turbulent flow is realized. For still further increases in $\dot{m}$, section CD moves up until point T is within the section limits (CD).

Under conditions of large $\dot{m}$, when section BC to CD is used, a liquid film of helium flows above the bushing top. The heat needed to vaporize this helium film is transferred from the outer bath to the inner helium film via conduction through the heat exchanger, H. In this way, large amounts of heat can be rejected (up to 1.5 W) without pure He-II convective heat transfer. Hence, pin design is important to the adaptability of the APS to specific applications. Section DE is required for pin guidance. The function of the ball closure, F, is to substantially reduce the mass flow when necessary, for example, during evacuation of a flooded heat exchanger after filling and topping off procedures (refs. 38 and 41). The ball closure is not leaktight to superfluids, however. The entire pin assembly itself is driven by an electromagnetic induction subassembly coupled to a bath temperature feedback control system. Experimental data have shown that $\dot{m}$ can be adjusted from near zero values to 90 mg/sec at high bath temperatures, $T_b = 2.1$ K. Mass-flow rates up to 35 mg/sec have been noted at bath temperatures of 1.6 K.

Experimental Results

Figure 18 shows the dynamic response of the APS for step functions of the bath input. Stabilization of ΔT across the phase separator after steady state is of the order of 0.1 mK (ref. 40). For decreased step inputs in the bath heater, the direction of the fountain effect is seen to be opposite to the desired direction, that is, a vector force acting in the downstream direction. This helps to reduce $\dot{m}$ and maintain a constant T_b. Evidently, at $t = 6$-8 min, a stabilized negative ΔT is observed, indicating a balance between the thermomechanical effect and the maximum closure position of the pin. The mass-flow rate $\dot{m}$ follows ℓ and ΔT, as might be expected, decreasing to approximately 10 mg/sec at maximum pin closure and a reversed

(negative) ΔT. No bath-temperature/time functions are given. It would be informative to know the bath temperature stability and time-response curves. Figure 18(b) shows ℓ and ΔT for a step input in $\dot{Q}_{ext}$ at constant $T_b = 2.02$ K and a constant $\Delta P = 13.9$ mbar. The same performance is observed as shown in figure 18(a). In addition, curves are indicated for gaseous He flow through the APS, while maintaining a stable bath temperature and stable ΔT.

Figure 19(b) shows $\dot{m}$ versus the gap length ℓ for constant T_b and ΔP. A monotonic increase in $\dot{m}$ with decreasing ℓ is observed, with an observed proportionality to ℓ^{-1}, as predicted by equation (16). Figure 19(a) shows log $\dot{m}$ versus ℓ. It can be seen that up to 100 mg/sec of helium can pass through the phase separator at 2.0 K. Also, $\dot{m}$ can be reduced to approximately 1.3 mg/sec at the same T_b.

Figures 20(a)-20(c) show $\dot{m}$ versus ΔP at different constant gap lengths, ℓ and T_b. The solid lines indicate calculations based on equation (16). In the laminar-flow regime, data are predicted well. For higher turbulent flow, there is a large difference between what is predicted and what is observed, indicating the possibility of other flow phenomena besides GM convection.

5. CONCLUSIONS

The conclusions of this survey can be summarized as follows:

1. Porous plugs can satisfactorily function as passive helium II liquid-vapor phase separators. Heat fluxes of the order of 10 mW/cm^2 ($\dot{m}/A_T$ of the order of 1 mg/sec) have been demonstrated for a 0.5-μm ($K_p = 10^{-9}$ cm^2) stainless steel plug.

2. Two regions of transport exist: a laminar region in which $d(\dot{m}/A_T)/d\Delta P$ is large and a turbulent region in which $d(\dot{m}/A_T)/d\Delta P$ can be as much as 2 orders of magnitude less.

3. The maximum heat flux is primarily limited by the maximum available pressure drop from the bath to a vacuum. It can be increased by enlarging the plug cross-sectional area A_T or the permeability K_p. The minimum q, however, will be increased, and subsequently breakthrough conditions must be considered with the latter.

4. Downstream pressure regulation to adjust for varying heat loads and bath temperatures shows promise. The use of a downstream heater to control the thermomechanical force, hence, $\dot{m}$, should not be dismissed as an alternative.

5. The active phase-separator can reject a larger dynamic heat load at lower bath temperatures. Heat rejection rates of up to 700 mW at 1.6 K and 2 W at 2.1 K have been demonstrated. System pin and heat-exchanger design can be tailored to specific performance requirements. Moving components in a cryogenic environment must be considered.

It is recommended that an in-house facility be designed and constructed to test the performance of porous-plug phase separation for application to SIRTF. Following are the specific areas for which more detailed knowledge is necessary.

1. Testing of large K_p plugs (10^{-9} cm^2 < K_p < 10^{-8} cm^2; pore size range from 2 to 10 μm) for the possibility of larger heat rejection rates and the study of the limitations imposed by breakthrough conditions.

2. The effects of superficial plug geometry, ℓ and A_T.

3. Downstream pressure regulation for dynamic system control of T_b, $\dot{Q}_{ext}$, and ΔP, and the design and implementation of a downstream feedback mechanism to maintain system stability.

4. Overall correlation of all obtainable data on plug performance into a common frame of reference to predict plug performance.

REFERENCES

1. Urbach, A. R.; and Mason, P. V.: IRAS Cryogenic System Flight Performance Report. Presented at the Cryogenic Engineering Conference, Colorado Springs, Colo., 1983.

2. Tisza, L.: Sur la Theorie des Liquides Quantiques: Application a l'Helium Liquids, I et II. J. Phys. Radium, vol. 1, 1940, pp. 164-172.

3. Landau, L. D.: Theory of the Superfluidity of Helium II. Phys. Rev., vol. 60, 1941, pp. 356-358.

4. Wilkes, J.: The Properties of Liquid and Solid Helium. Clarendon, Oxford, 1967.

5. Putterman, S. J.: Superfluid Hydrodynamics. Elsevier, N.Y., 1974.

6. Landau, L. D.; and Liftschitz, E. M.: Fluid Mechanics. Pergamon, London, 1959.

7. London, H.: Thermomechanical Effect of Liquid He II. Proc. R. Soc. of London, Sect. A, vol. 171, 1939, pp. 484-496.

8. Gorter, C. J.; and Mellink, J. H.: On the Irreversible Processes in Liquid Helium II. Physica, vol. 15, 1949, pp. 285-304.

9. Frederking, T. H. K.; van Kempen, H.; Weenen, M. A.; and Wyder, P.: Critical Counterflow in Narrow He-II-Filled Channels. Physica, vol. 108B, 1981, pp. 1129-1130.

10. Soloski, S. C.; and Frederking, T. H. K.: Dimensional Analysis and Equation for Axial Heat Flow of Gorter-Mellink Convection (He II). Int. J. Heat Mass Transfer, vol. 23, 1980, pp. 437-441.

11. Tough, J. T.: Superfluid Turbulence. Progress in Low Temperature Physics VIII. North-Holland Publ. Co., 1982, pp. 133-219.

12. Martin, K. P.; and Tough, J. T.: Evolution of Superfluid Turbulence in Thermal Counterflow. Phys. Rev. B, vol. 27, no. 5, 1983, pp. 2788-2799.

13. Dimotakis, P. E.: Gorter-Mellink Scale and Critical Velocities in Liquid Helium II Counterflow. Phys. Rev. A, vol. 10, no. 5, 1974, pp. 1721-1723.

14. Schotte, U.: The Physics of He II Phase Separation. Physica, vol. 107B, 1981, pp. 577-578.

15. Schotte, U.: Flow States and Heat Transfer Properties of He II Phase Separators. Adv. in Cryo. Eng., vol. 27, 1981, pp. 421-430.

16. Schotte, U.; and Denner, H. D.: The Mechanism Governing Phase Separation of Helium II by Means of Narrow Channels. Proceedings of the 8th International Cryogenics Engineering Conference, Genoa, Italy, 1980, pp. 27-31.

17. Hendricks, J. G.; and Karr, G. R.: Characterization of Superfluid Porous Plug Performance. Proceedings of the 9th International Cryogenic Engineering Conference, Kobe, Japan, 1982, pp. 190-193.

18. Hendricks, J. B.; and Karr, G. R.: Superfluid Porous Plug Performance. Presented at the Cryogenic Engineering Conference, Colorado Springs, Colo., 1983.

19. DiPirro, M.; Fash, F.; and McHugh, D.: Precision Measurements on a Porous Plug for Use in COBE. Space Helium Dewar Conference and Workshop, NASA Marshall Space Flight Center, Huntsville, Ala., 1983.

20. DiPirro, M.: The Operation of Porous Plug in Cobe and IRAS Dewars. NASA Report X-713-82-4, 1981.

21. Karr, G. R.; and Urban, E. W.: Superfluid Plug as a Control Device for Helium Coolant. Cryogenics, May 1980, pp. 266-270.

22. Donnelly, R. J.: Experimental Superfluidity. U. of Chicago Press, 1967.

23. Yuan, S. W. K.: The Characterization of Sintered Stainless Steel Porous Plugs for Vapor-Liquid Phase Separation of He II. Master thesis, U. of California at Los Angeles, 1981.

24. Yuan, S. W. K.; and Frederking, T. H. K.: Darcy Law of Thermo-osmosis for Zero Net Mass Flow at Low Temperatures. Proceedings of the Thermal Engineering Joint Conference of the ASME-JSME, Honolulu, Hawaii, vol. 2, 1983, pp. 191-197.

25. Lee, J. M.; Yuan, S. W. K.; and Frederking, T. H. K.: The Zero Net Asymptote to Thermo-osmotic Vapor-Liquid Phase Separation. Chemical Eng. J. (submitted, 1983).

26. Yuan, S. W. K.; Lee, J. M.; Kamioka, Y.; and Frederking, T. H. K.: Plug Flow Comparison. Space Helium Dewar Conference and Workshop, NASA Marshall Space Flight Center, Huntsville, Ala., 1983.

27. Lee, J. M.: Permeabilities of Sintered Porous Metal Plugs and Transport Rates of Vapor-Liquid Phase Separators for Helium II Vessels. Master thesis, U. of California at Los Angeles, 1983.

28. Petrac, D.; and Mason, P. V.: Temperature Control of Superfluid Helium in Zero-g by a Porous Plug. Proceedings of the 8th International Cryogenic Engineering Conference, Genoa, Italy, 1980, pp. 97-101.

29. Denner, H. D.; Klipping, G.; Klipping, I.; Menzel, J.; and Rupert, U.: Flow of Helium II through Porous Plugs. Cryogenics, vol. 18, 1978, pp. 166-170.

30. Soloski, S. C.: Thermomechanical Gorter-Mellink Convection of Liquid Helium II in a Duct with Zero and Finite Angular Velocities, and the Influence of Interfacial Instability upon a Heated Helium II Boundary Layer. Ph.D. dissertation, U. of California at Los Angeles, 1977.

31. Frederking, T. H. K.; Chuang, C.; Kamioka, Y.: Lee, J. M.; and Yuan, S. W. K.: Sintered Plug Flow Modulation of a Vapor-Liquid Phase Separator for a Helium II Vessel. Presented at the Cryogenic Engineering Conference, Colorado Springs, Colo., 1983.

32. Petrac, D.; and Mason, P. V.: Evaluation of Porous Plug Liquid Separators for Space Superfluid Helium Systems. Proceedings of the 7th International Cryogenic Engineering Conference, London, England, 1978, pp. 120-125.

33. Petrac, D.: Superfluid Porous Plug as a Liquid-Vapor Separator in Low-Gravity Space Flights. Proceedings of the 14th International Conference on Low Temperature Physics, Helsinki, 1975, pp. 33-36.

34. Murakami, M.; Nakaniwa, N.; and Uyama, K.: Porous Plug Phase Separator for Superfluid He II. Proceedings of the 9th International Cryogenic Engineering Conference, Kobe, Japan, 1982, pp. 194-197.

35. Urban, E. W.; and Katz, L.: Helium II Flow Through and Vapor Separation by Porous Plugs. Proceedings of the 14th International Conference on Low-Temperature Physics, Helsinki, 1975, pp. 37-40.

36. Scheidegger, A. E.: The Physics of Flow through Porous Media. Third ed., University of Toronto Press, Toronto, 1974.

37. Dullien, F. A.: Porous Media Fluid Transport and Pore Structure. Academia Press, N.Y., 1979.

38. Denner, H. D.; Klipping, G.; Klipping, I.; Lüders, K.; Oesterlick, T.; Ruppert, U.; Schmedtchen, U.; Szücs, Z.; and Walter, H.: Improved Active Phase Separator for He II Space Cooling Systems. Adv. Cryo. Eng., vol. 27, 1981, pp. 1079-1086.

39. Denner, H. D.; Klipping, G.; Klipping, I.; Lüders, K.; Menzel, J.; and Ruppert, U.: Mechanism of an Active Phase Separator for Space Applications. Adv. Cryo. Eng., vol. 25, 1979, pp. 783-790.

40. Denner, H. D.; Klipping, G.; Klipping, I.; Lüders, K.; Menzel, J.; and Ruppert, U.: Performance of an Active Phase Separator. Proceedings of the 8th International Cryogenics Engineering Conference, Genoa, Italy, 1980, pp. 32-37.

41. Henner, H. D.; Klipping, G.; Klipping, I.; and Schmidtchen, U.: Stability of He II Phase Separation — Investigations with the Active Phase Separator. Presented at the Cryogenic Engineering Conference, Colorado Springs, Colo., 1983.

TABLE 1.- POROUS-PLUG TEST DATA

Plug number	Plug and pore,[a] μm	Nominal size,[b] μm	$K_{p_{T_{room}}}$, cm^2	Area, cm^2	Thickness, cm	ε	Material	Reference	Bonding	Experiment[c]	F-factor,[d] g/(dyne·sec)	Comments
1	M,f,0.5	3.92-b	9.6×10^{-10}	25	0.61		Stainless	(e)		PT		(f),(g)
2	M,f,0.5	3.92-b	1.24×10^{-9}	25	.61		Stainless	(e)		PT		(f),(g)
3	M,f,0.5	3.92-b	1.04×10^{-9}	25.3	.61		Stainless	(e)		PT		(f),(g)
4	M,f,0.5	3.92-b	1.03×10^{-9}	4.7	.61		Stainless	(e)		PT		(g),(h)
5	M,f,0.5	3.92-b	1.07×10^{-9}	3.5/3.0[i]	.61		Stainless	(e)	BASD[j]	PS		Final IRAS plug[g]
6	M,f,0.5			1.27	0.64		Stainless	17		PS		
7	M,f,2			5.07	.318	0.31	Stainless	27	Stycast 1266	ZNMF		M2511[k]
8	M,f,2			5.07	.318	.309	Stainless	27		PS		M2S2[k]
9	M,f,2		5.59×10^{-9}	5.07	.318	.314	Stainless	27	Stycast 1266	PT		M2S3[k]
10	M,f,5	25-30-b	1.87×10^{-8}	25.3	.64		Stainless	(e)	RTV-180	PT		Original IRAS plug
11	M,f,5		3.1×10^{-8}	5.07	0.318	0.346	Stainless	27	Stycast 1266	PT		
12	P,f,2-5		5.5×10^{-10}	4.7[l]	.67	.18	Stainless	28		PS		
13	P,f,2-5		5.59×10^{-9}	5.07	.318	.366	Stainless	27	Stycast 1266	PT		
14	P,f,5-15		1.05×10^{-7}	5.07	.636	.36	Bronze	27	Stycast 1266			
15	P,f,5-15		8.5×10^{-8}				Bronze	(m)				
16	C,7-10	7-10	1.26×10^{-8}	20	0.64	0.61	Al_2O_3	33		PT/PS	1.7×10^{-7}	
17	B,4		4.9×10^{-9}(n)	0.26	.64	3×10^{6}(o)	Stainless	28		PT/PS	3.9×10^{-6}	(p)
18	H,1		1×10^{-11}	10.18	.5	0.4	Al-Si	29		PS		
19	S,9-11		3.4×10^{-9}	10.18	.4	.4	Glass	29		PS		
20	5		5×10^{-10}	15.1	.65	.52	Al_2O_3	21	Epoxy	PS		
21	M			12.97	0.64/1.91		Stainless	19		PS		COBE
22	Fab.	2	3.5×10^{-10}	1.96	.15		Stainless	34		PS		
23	Fab.	10	1.2×10^{-9}	3.80	.7		Ceramic Al_2O_3	34		PS		
24	Fab.	10	9.4×10^{-10}	3.80	1.0		Ceramic Al_2O_3	34		PS		
25	10		3.77×10^{-9}	15.1	.63	0.384	Nickel	35		PS		(q)
26	10		2.24×10^{-9}	15.1	0.66	0.677	Al_2O_3	35		PS		(q)
27	0.5		5.73×10^{-11}	15.1	.65	.548	Al_2O_3	35		PS		(q)
28	C	<0.5-b		3.6	.64			32			1.5×10^{-8}	
29	Py 36060	2-2.5		6	.02			32			2.9×10^{-7}	
30	T,15fine	<3		1.8	.64			32			1.1×10^{-6}	

[a] M = Mott Metallurgical Co.; f = filtration grade; PSM = Pacific Sintered Metals; C = Coors; B = Brunswick; H = Haldenwanger (Berlin); S = Schott; Fab = fabricated by study investigator; Py = Pyrex; T = Tetraglass. [b] Values measured by the investigator; suffix "b" indicates bubble pressure test. [c] PT = permeability test; PS = phase separation; ZNMF = zero net mass flow. [d] F-factor defined by equation (29). [e] D. Petrac 1979: unpublished report. [f] Phase separator for powers >0.3 W. [g] Minimum steady-state cooling power 6-8 mW/cm^2. [h] Phase separation at 44 mW not possible. [i] 3.5 upstream, 3.0 downstream, owing to location of thermometer. [j] BASD = Ball Aerospace Division Specification BPS 11.08. [k] Plug designation by investigator. [l] From reference 15. [m] T. H. K. Frederking 1984: personal communication. [n] At low temperature. [o] Tubes per square centimeter. [p] Collimated capillary structure with 750,000 capillaries. [q] Graphs flow rate versus T_b with T_u and T_d at various heat inputs.

TABLE 2.- TIME-CONSTANTS FOR A TRANSIENT HEATING EXPERIMENT — HEATERS LOCATED UPSTREAM OF AND DOWNSTREAM FROM A 5-μm POROUS PLUG [from ref. 21]

Power, mW	b_1, min^{-1}	P_1, Torr	b_2, min^{-1}	P_2, Torr
Liquid heater				
362	0.295	14.1	0.302	3.05
285	.287	12.3	.270	3.81
Plug heater				
45.3	0.33	4.83	0.479	3.43
101	.412	6.46	.392	3.33
178	.515	8.97	.476	3.71
276	.603	12.21	.587	3.78
304	.720	13.04	.637	3.71
381	.769	15.1	.774	3.14
400.9	.861	16.0	1.067	3.43
465	.714	17.1	.509	4.57
Full power ≈ 1000	1.02	32.3	1.00	4.57

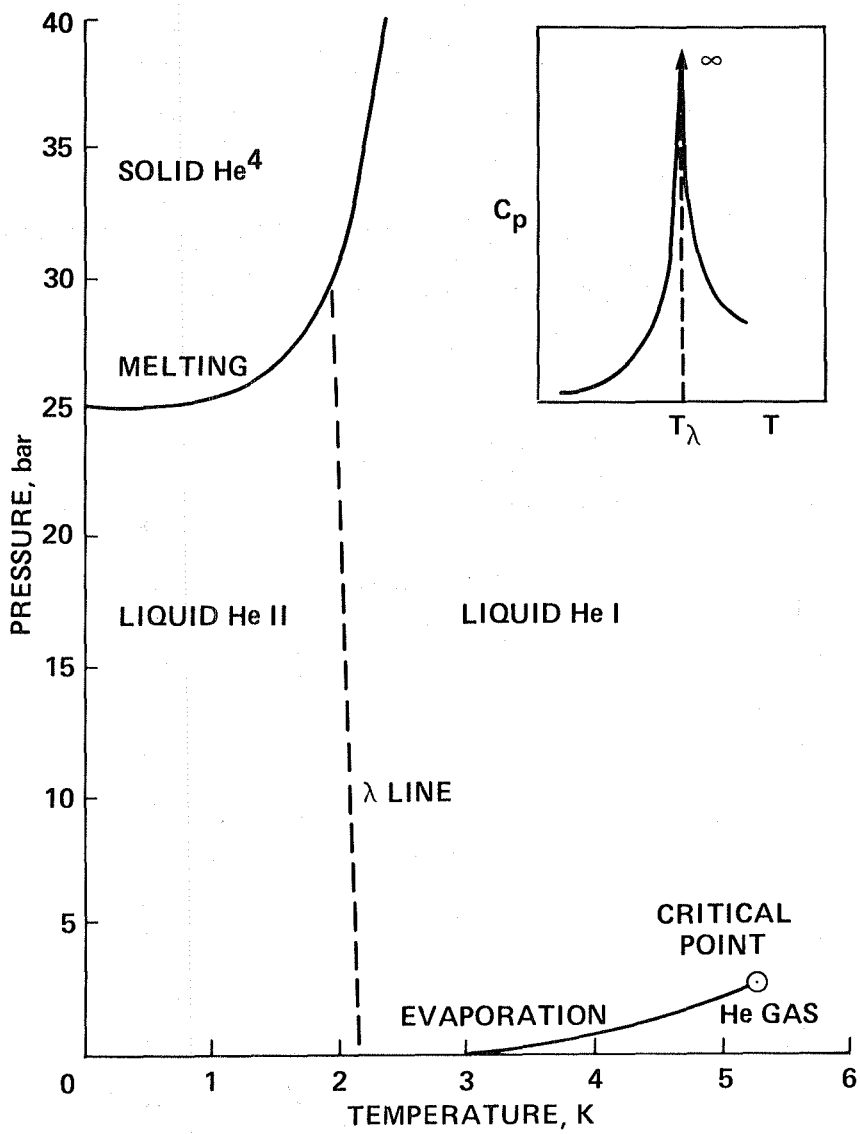

Figure 1.- Phase diagram of helium. Inset: heat capacity as a function of temperature.

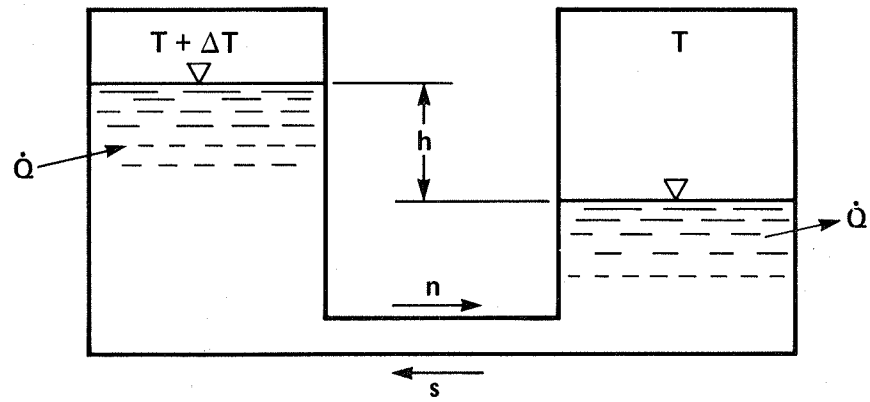

Figure 2.- Zero net mass flow: at steady state, the fountain pressure is checked by the pressure head, i.e., $\Delta P_T = \rho gh$ (n and s represent the flow directions of the normal fluid and superfluid components, respectively).

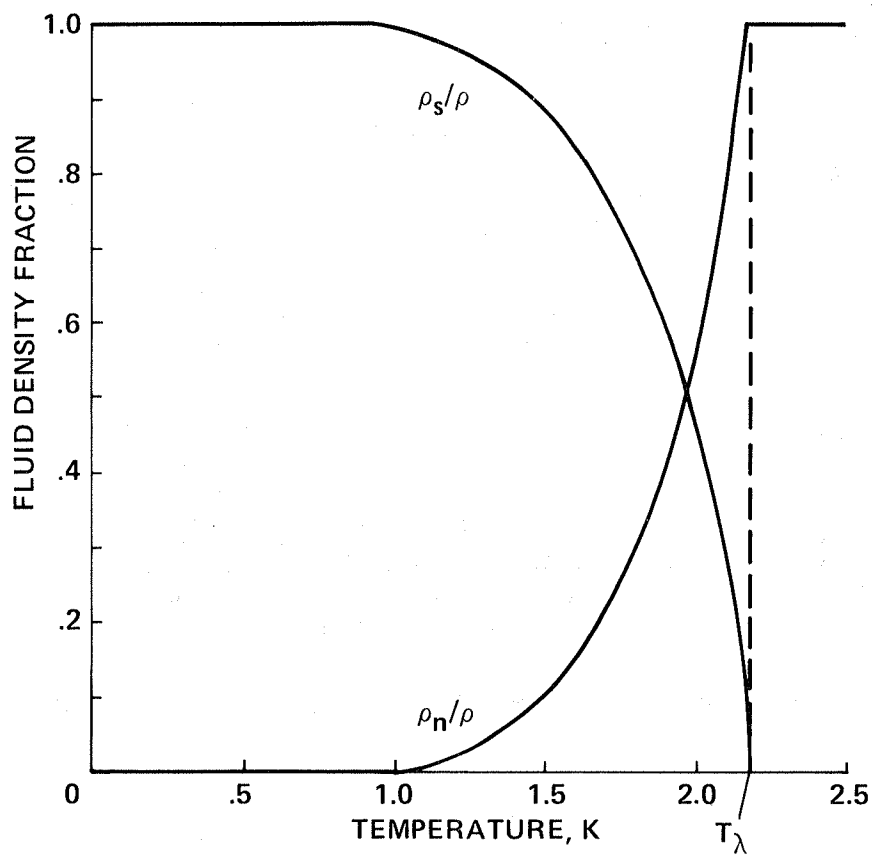

Figure 3.- Superfluid and normal fluid density ratio dependence on temperature.

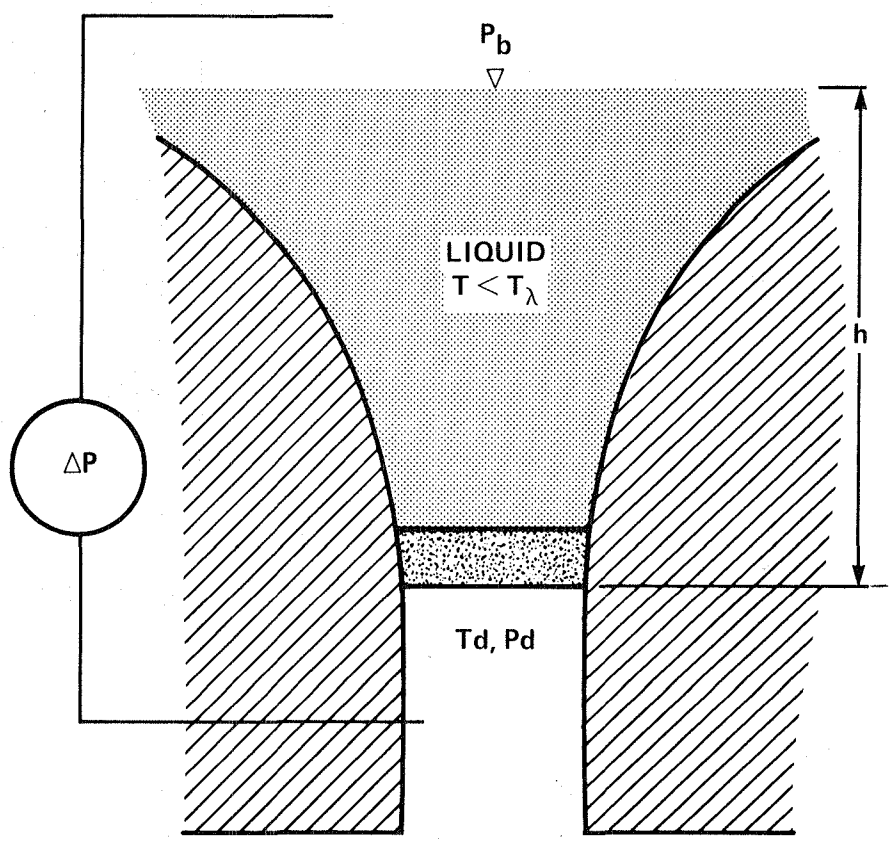

Figure 4.- General conditions for He-II phase separation: $\Delta P_T > \Delta P + \rho gh$; $T_b < T_d < T_\lambda$.

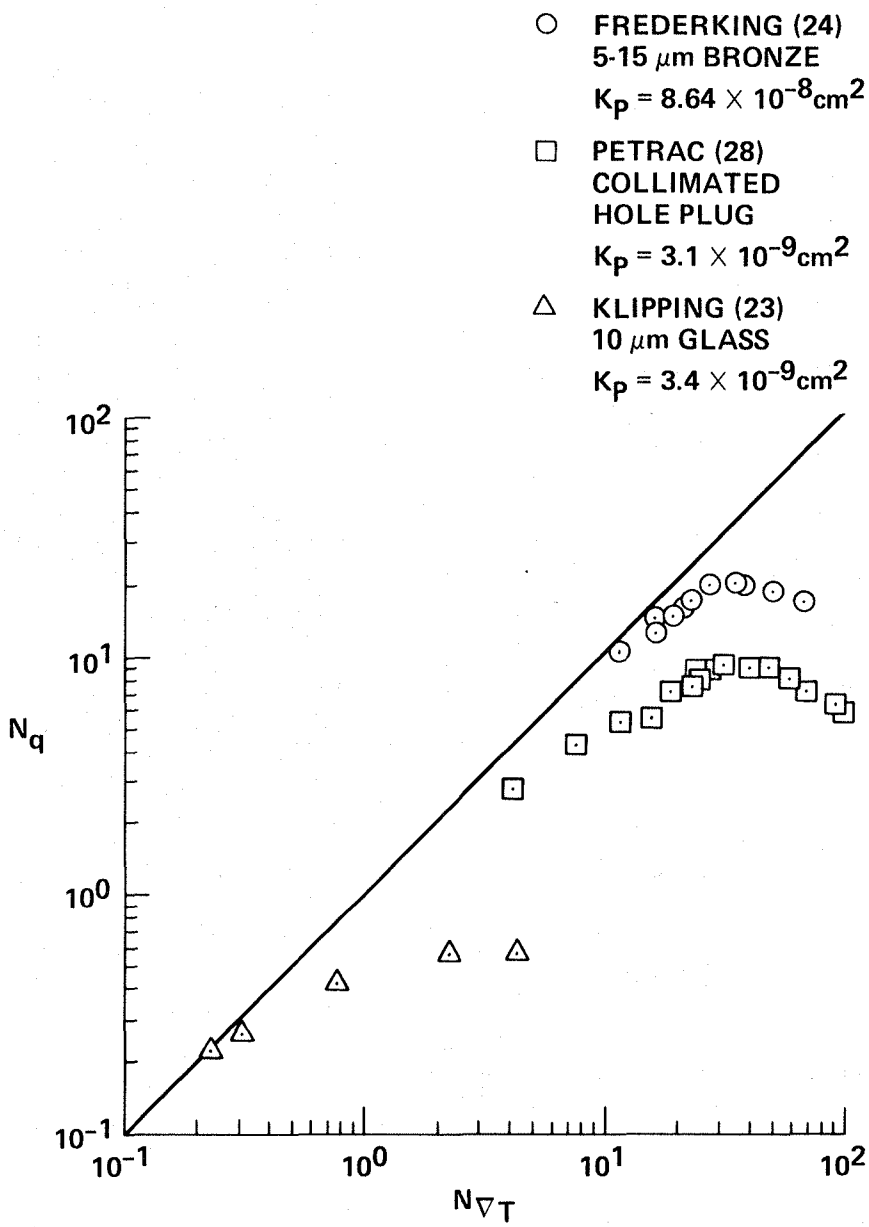

Figure 5.- Phase-separation data approaching conditions of zero net mass flow as T_b decreases; solid line represents the asymptotic limit to the thermo-osmotic Darcy equation, $N_q = N_{\nabla T}$ (T. H. K. Frederking 1984: personal communication).

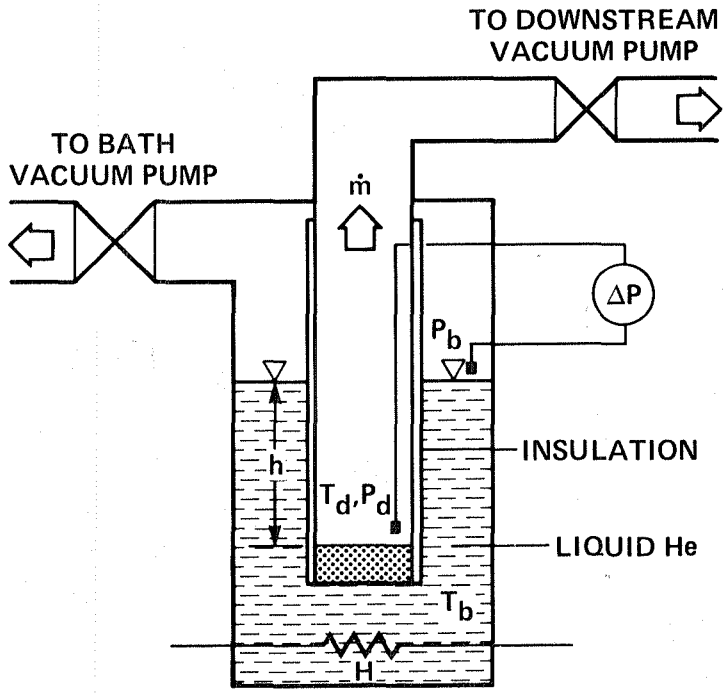

Figure 6.- Schematic of a porous-plug testing apparatus for He-II vapor-liquid-phase separation.

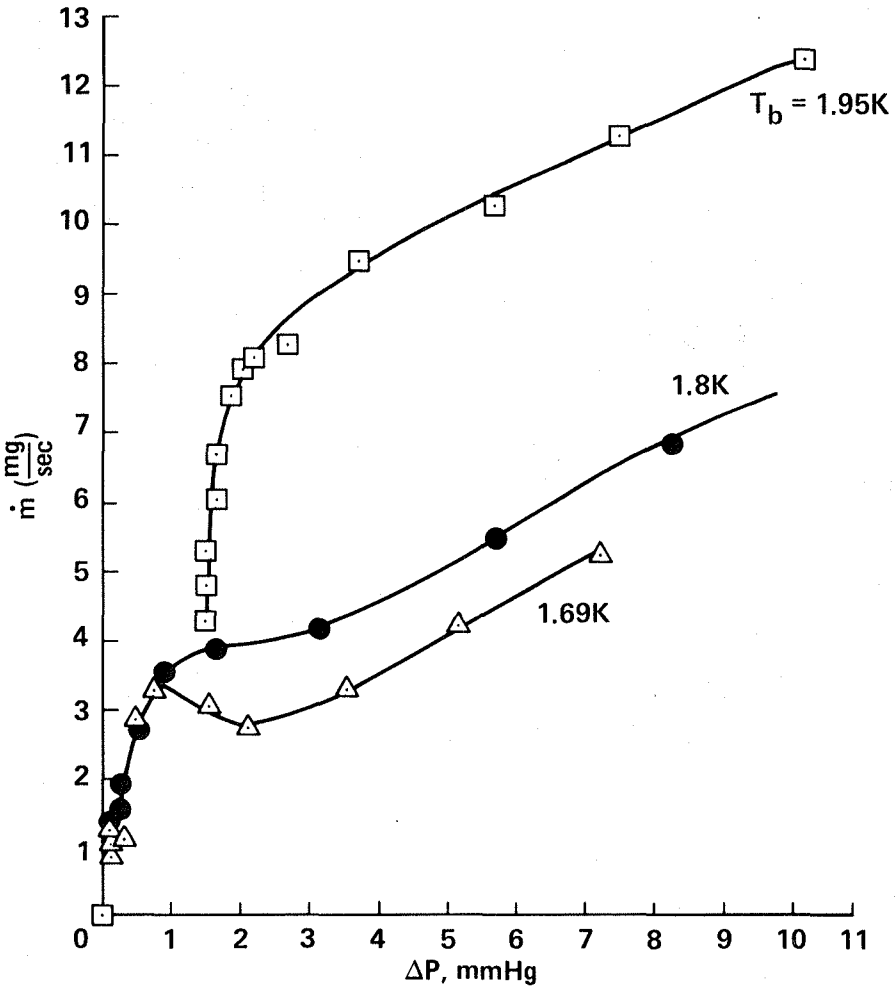

(a) $\dot{m}$ vs ΔP phase separation of in-flight IRAS porous plug: 0.5-μm Mott plug, $K_p = 1 \times 10^{-9}$ cm^2 (D. Petrac 1979: unpublished report).

Figure 7.- Measured parameters during phase-separation experiments.

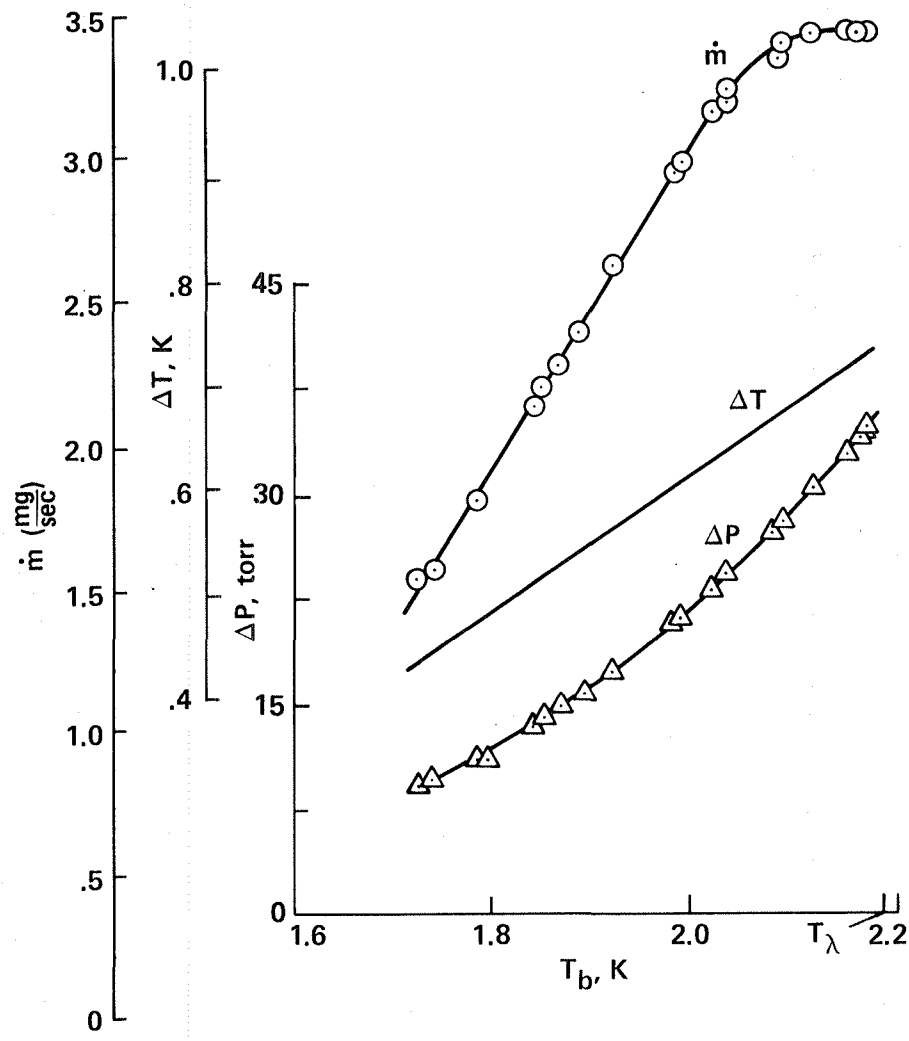

(b) $\dot{m}$, ΔP, ΔT vs T_b at constant downstream pump impedance (ref. 29).

Figure 7.- Concluded.

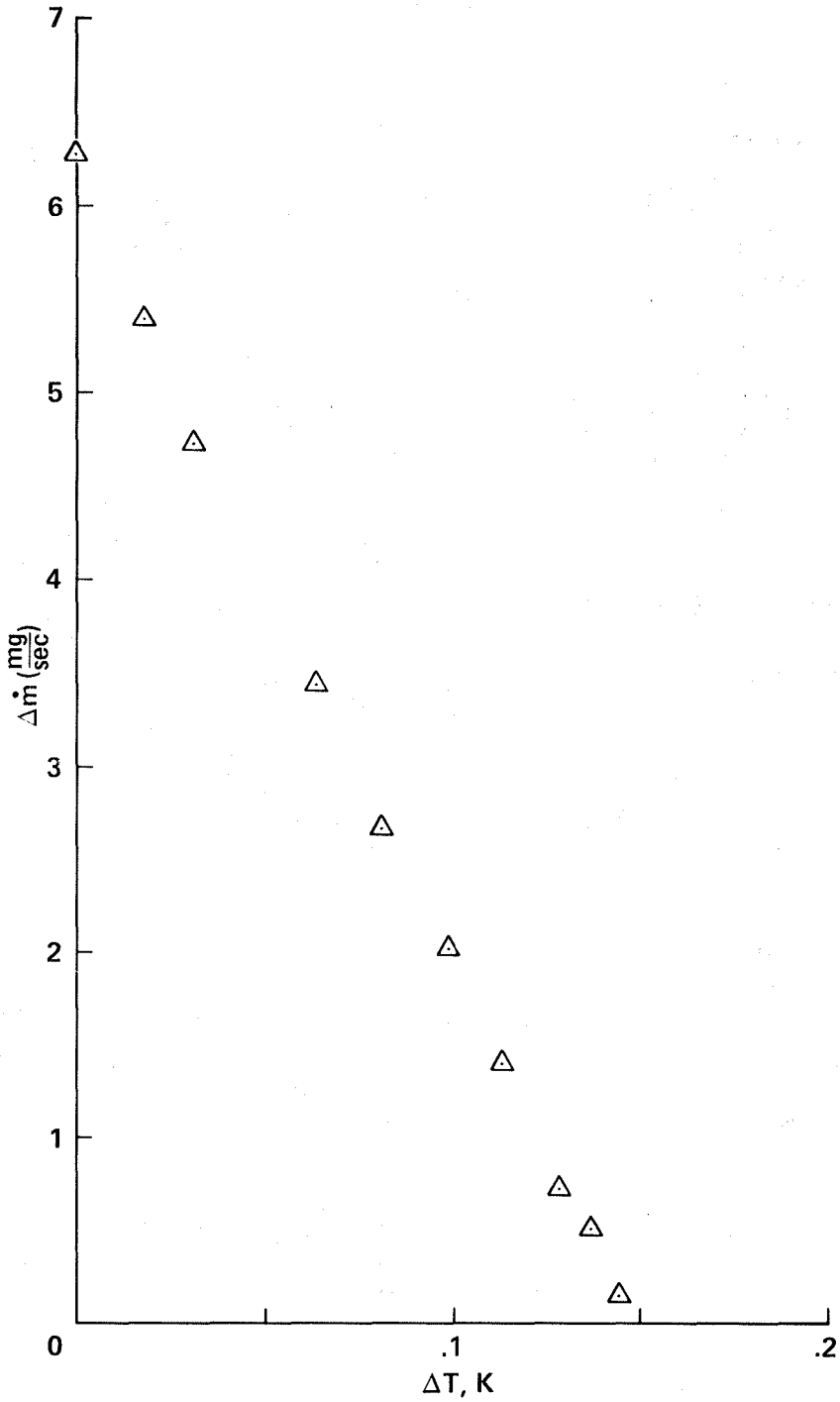

Figure 8.- Mass-flow variation using a downstream heating element across a 10-μm ceramic alumina porous plug: $\Delta\dot{m} = \dot{m} - \dot{m}_{\dot{Q}_{ext}=0}$ (ref. 34).

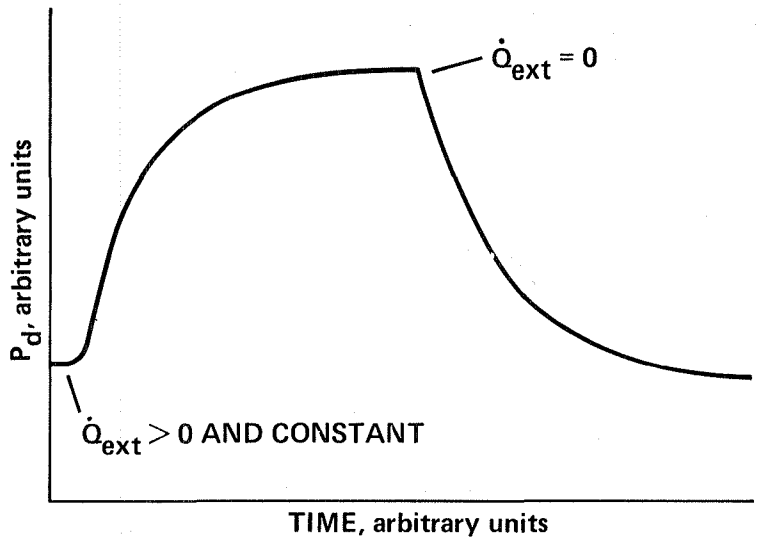

Figure 9.- Transient response of the downstream pressure when a step in power is applied to a heater located downstream from a porous plug (ref. 21).

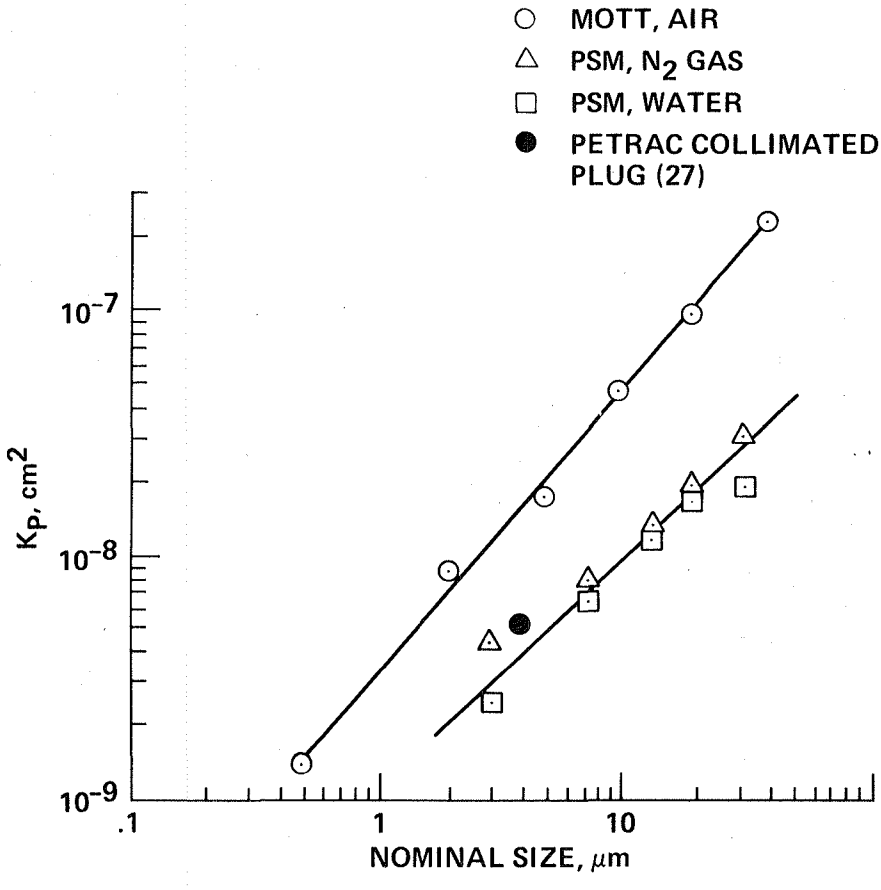

Figure 10.- Room temperature permeability vs manufacturer's stated nominal size; Mott and PSM size measurements by filtration.

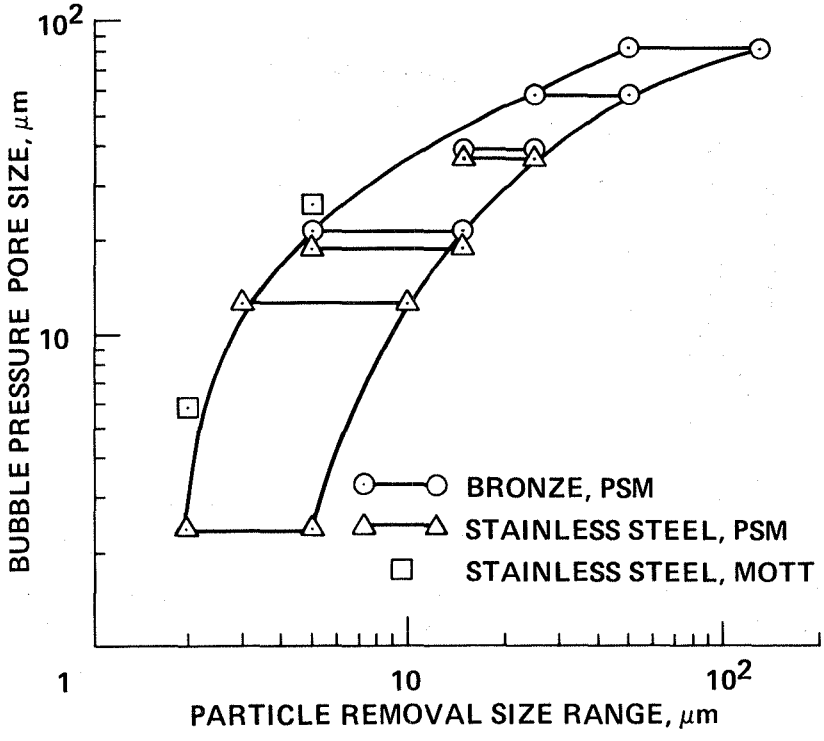

Figure 11.- Bubble pressure pore size vs particle removal size range for Mott and PSM porous plugs.

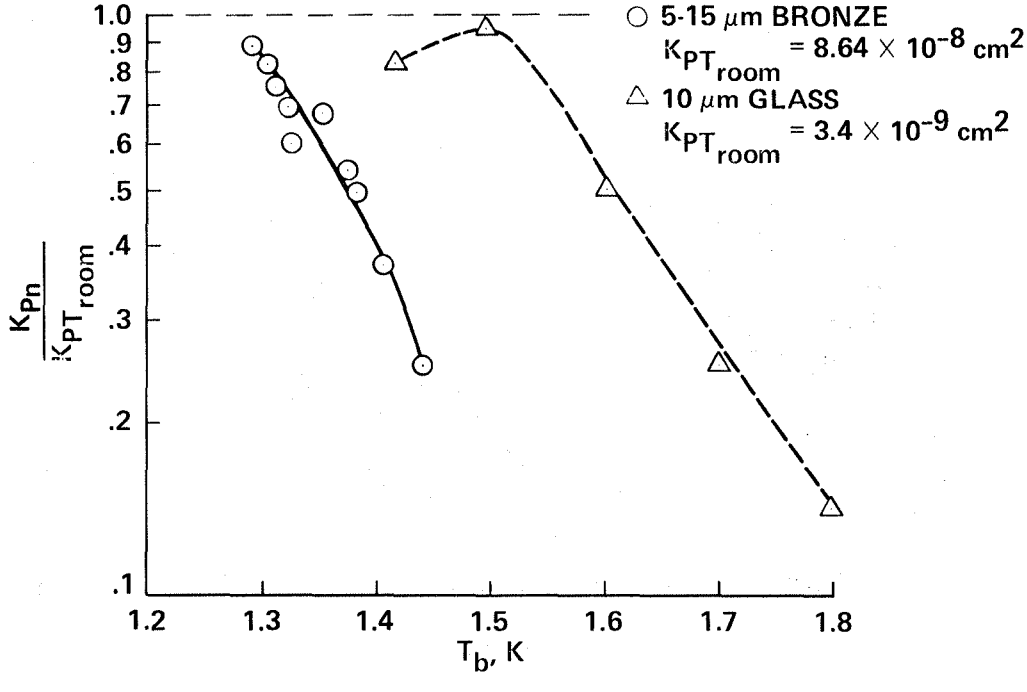

Figure 12.- $K_{pT_{room}}$ vs T_b showing K_{p_n} approaching $K_{pT_{room}}$ at the low temperature asymptote to zero net mass flow.

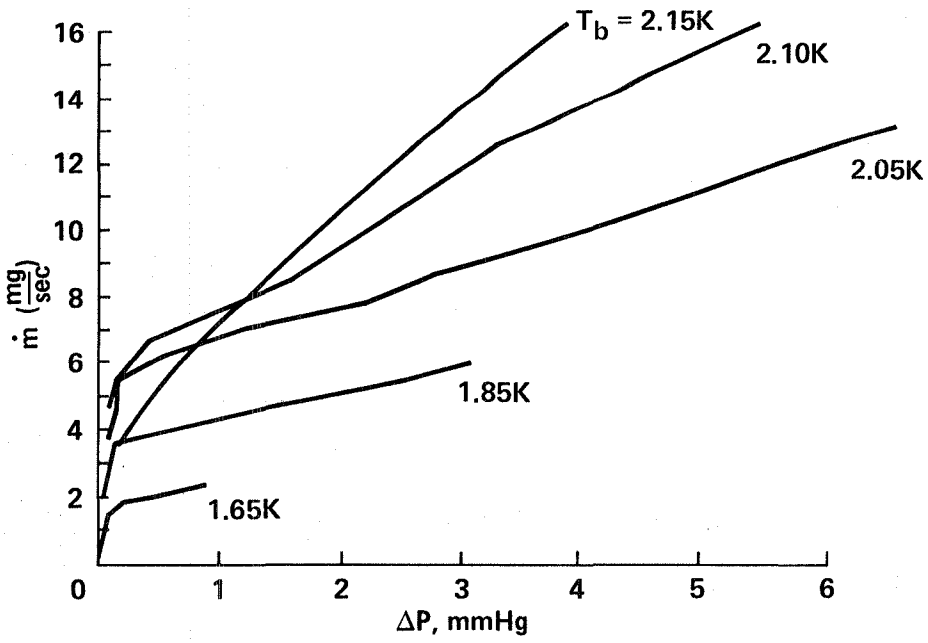

Figure 13.- Mass-flow rate vs pressure drop across a 0.5-μm stainless steel porous plug (ref. 17).

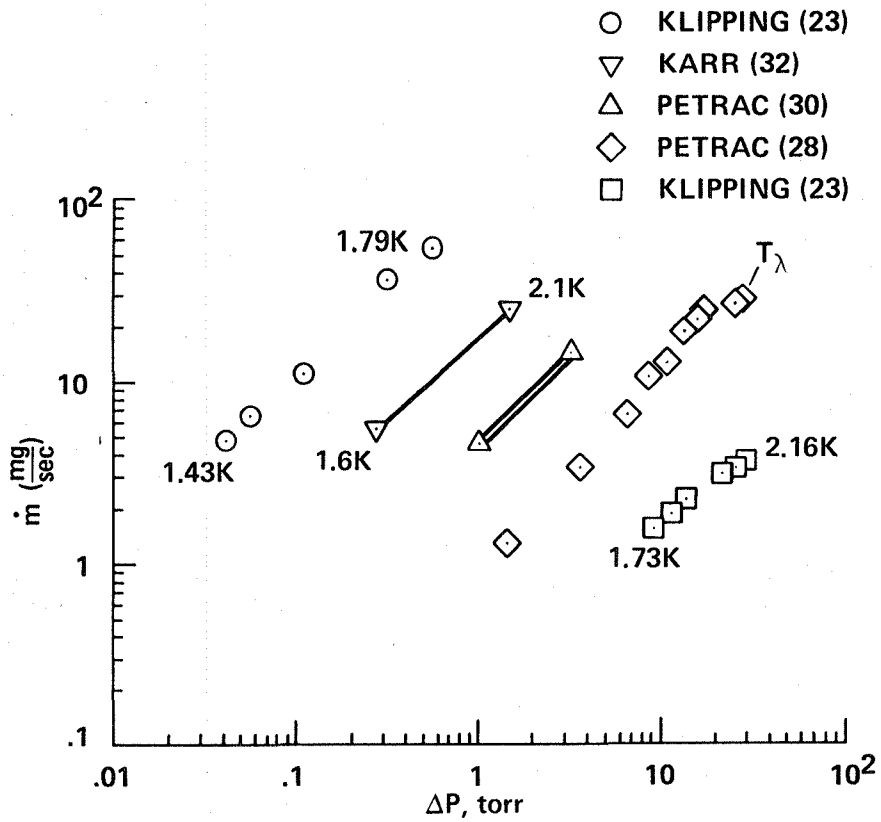

Figure 14.- Mass-flow rate vs pressure drop for a variety of porous plugs: K_p range = 10^{-11} cm^2 to 10^{-9} cm^2; pore size range = 1 to 10 μm.

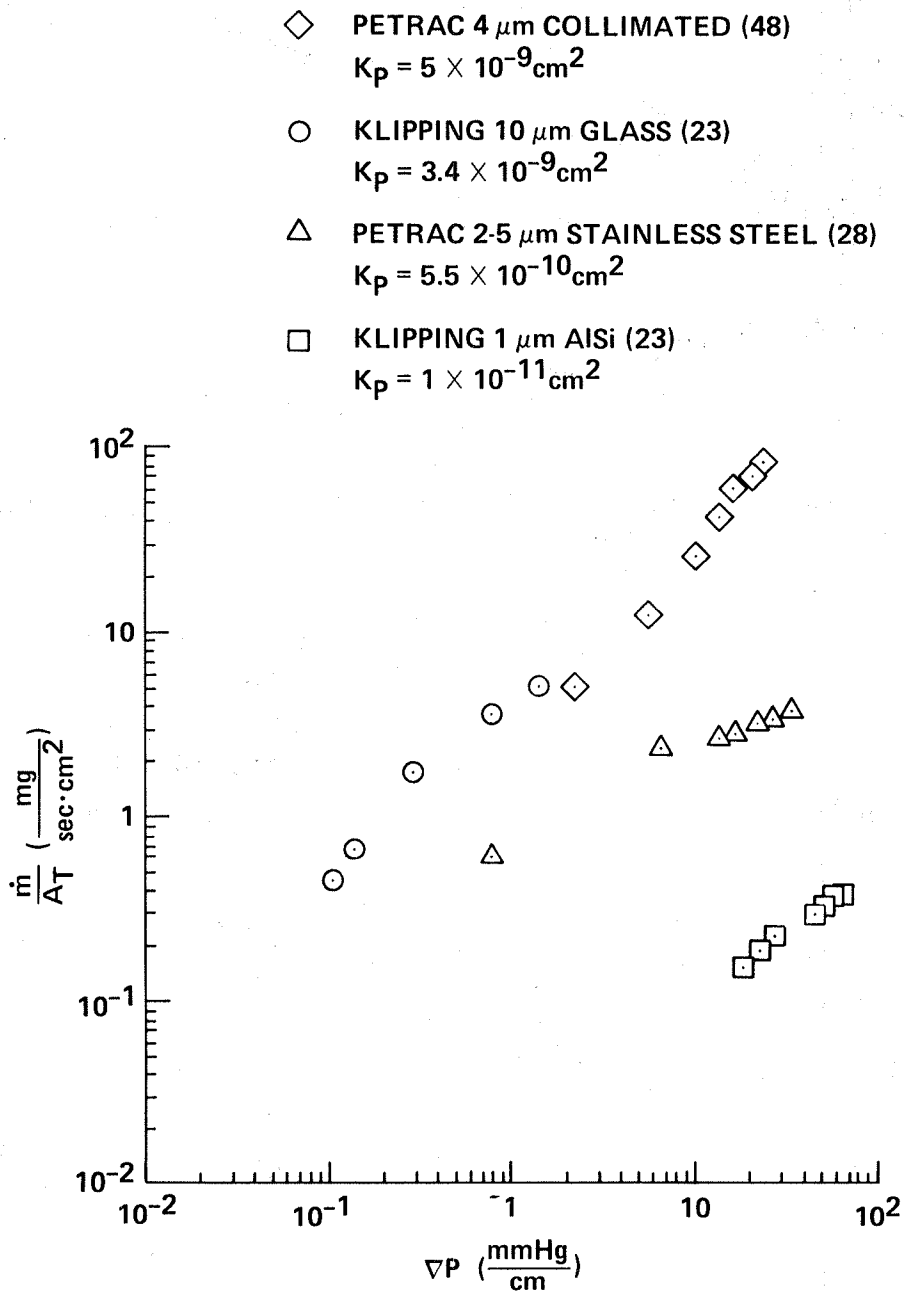

Figure 15.- Mass-flux density vs pressure gradient for porous media with 10^{-11} cm^2 < K_p < 10^{-9} cm^2.

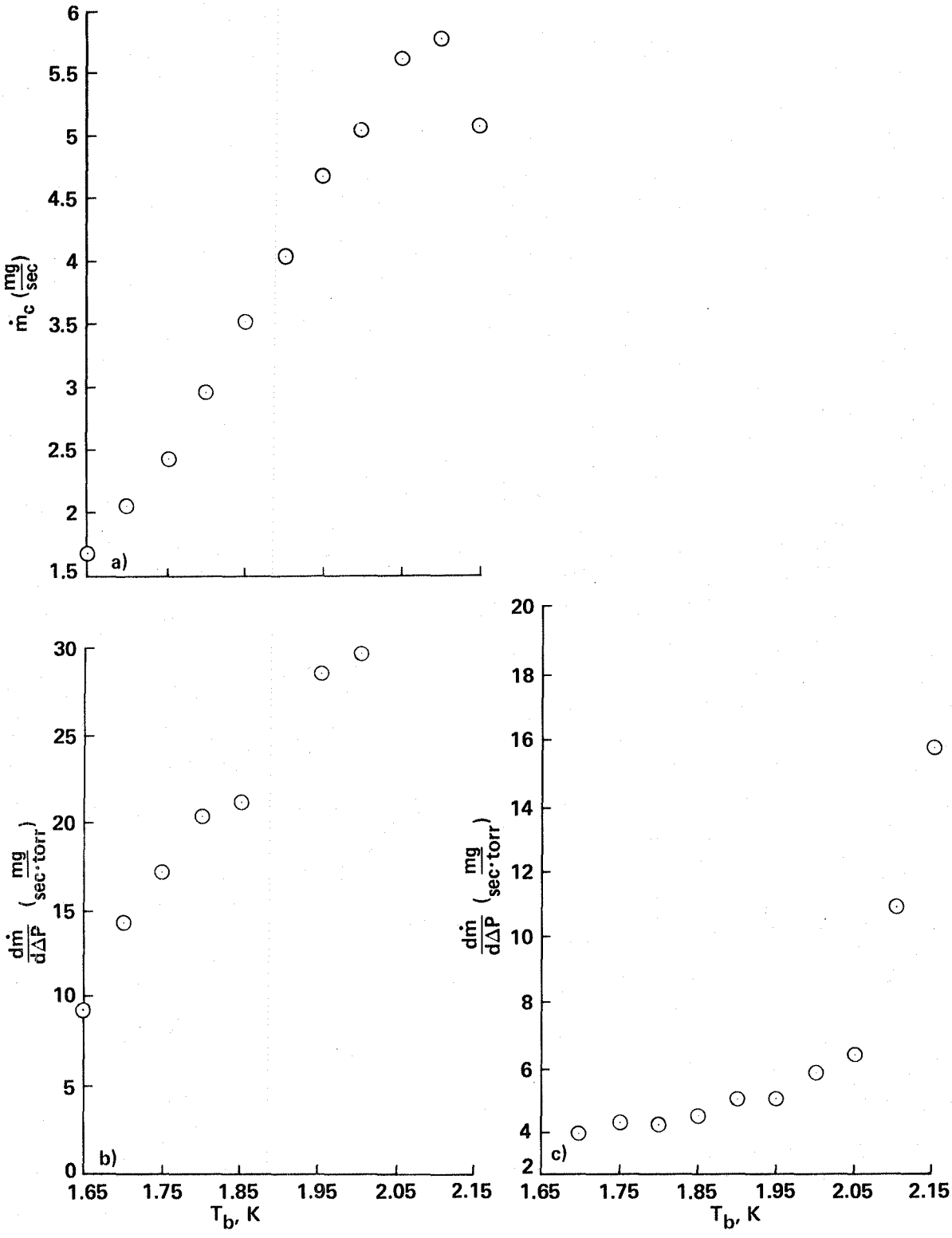

Figure 16.- Performance of a 0.5-μm Mott plug; No. 6 in table 1 (ref. 17). a) Mass-flow rate transition vs bath temperature. b) $d\dot{m}/d\Delta P$ vs T_b for laminar flow. c) $d\dot{m}/d\Delta P$ vs T_b for turbulent flow.

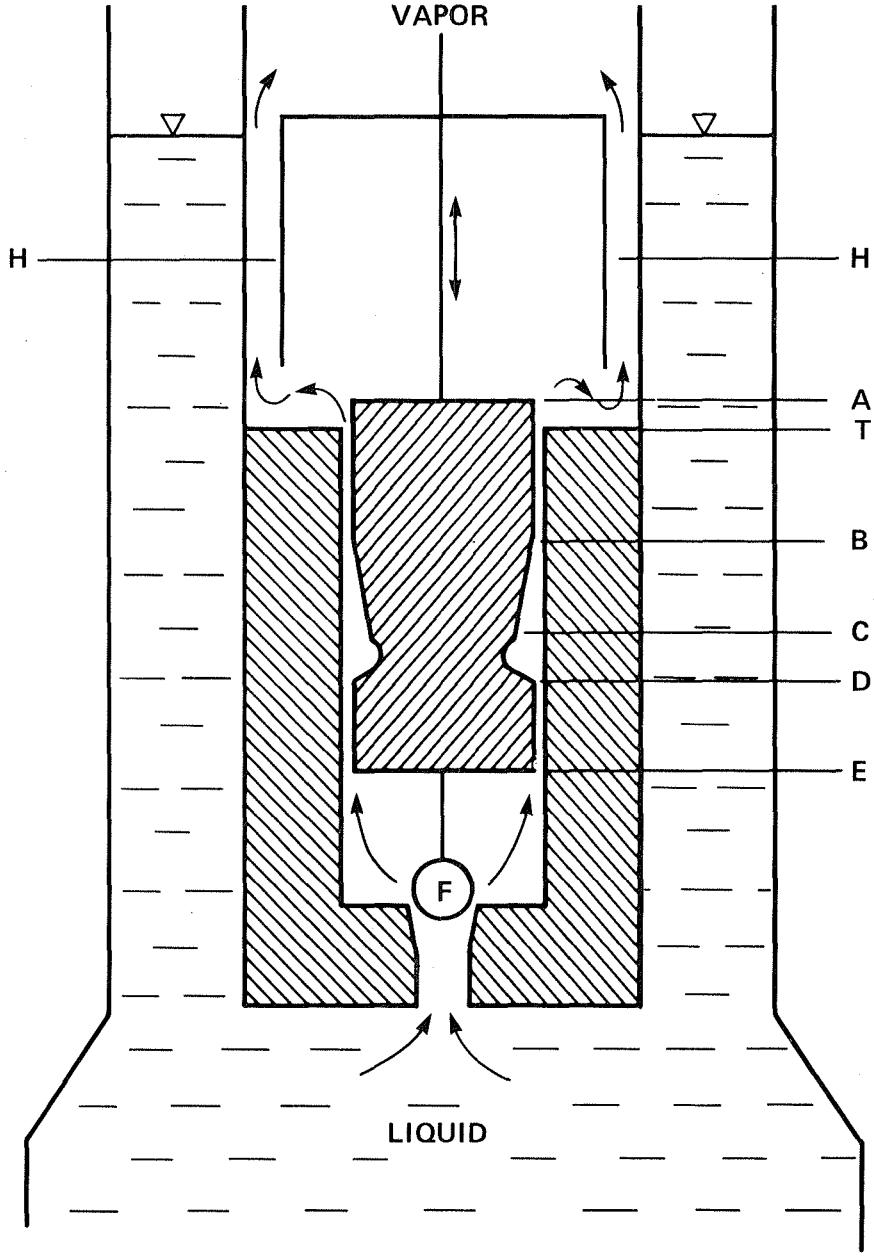

Figure 17.- Schematic of the active phase separator.

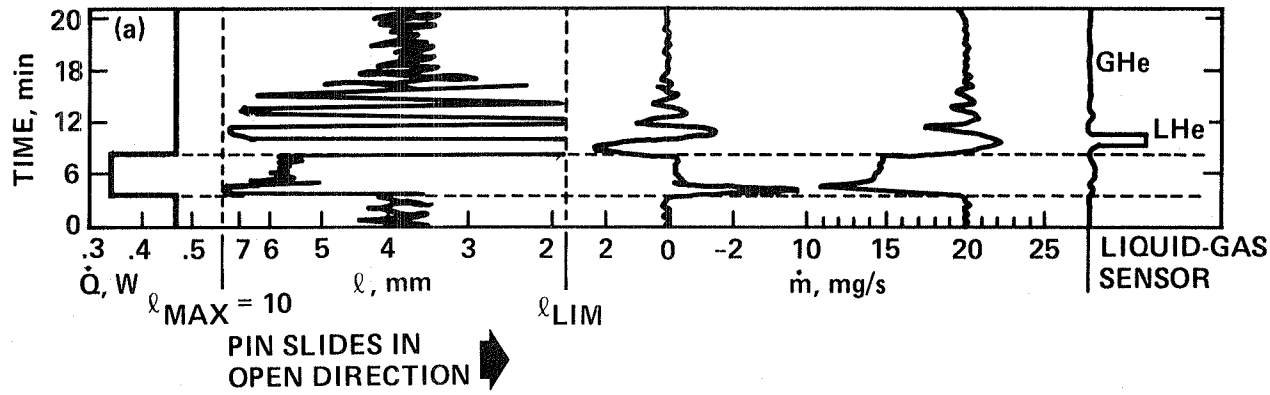

(a) T_b = 1.602 K, ΔP = 3.7 mbar.

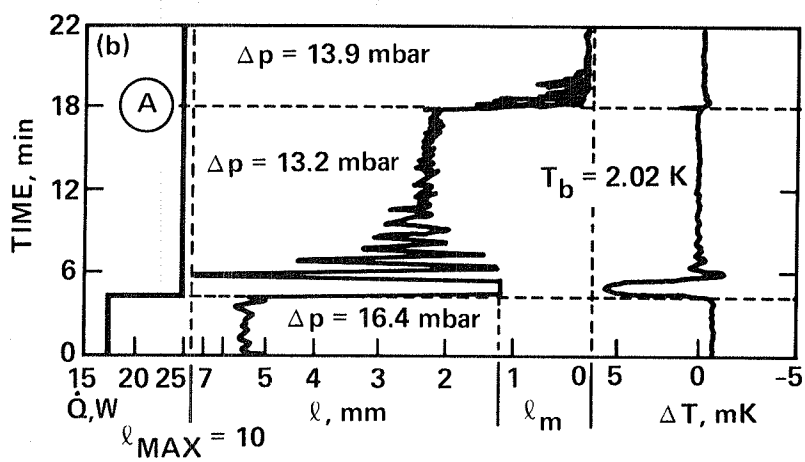

(b) T_b = 2.012 K; ΔP = 13.2 mbar with liquid in contact with APS; ΔP = 13.9 mbar with only cold helium gas flowing through APS.

Figure 18.- Dynamic response of the active phase separator (ref. 21): ΔT and $\dot{m}$ as a function of ℓ for step inputs in $\dot{Q}_{ext}$.

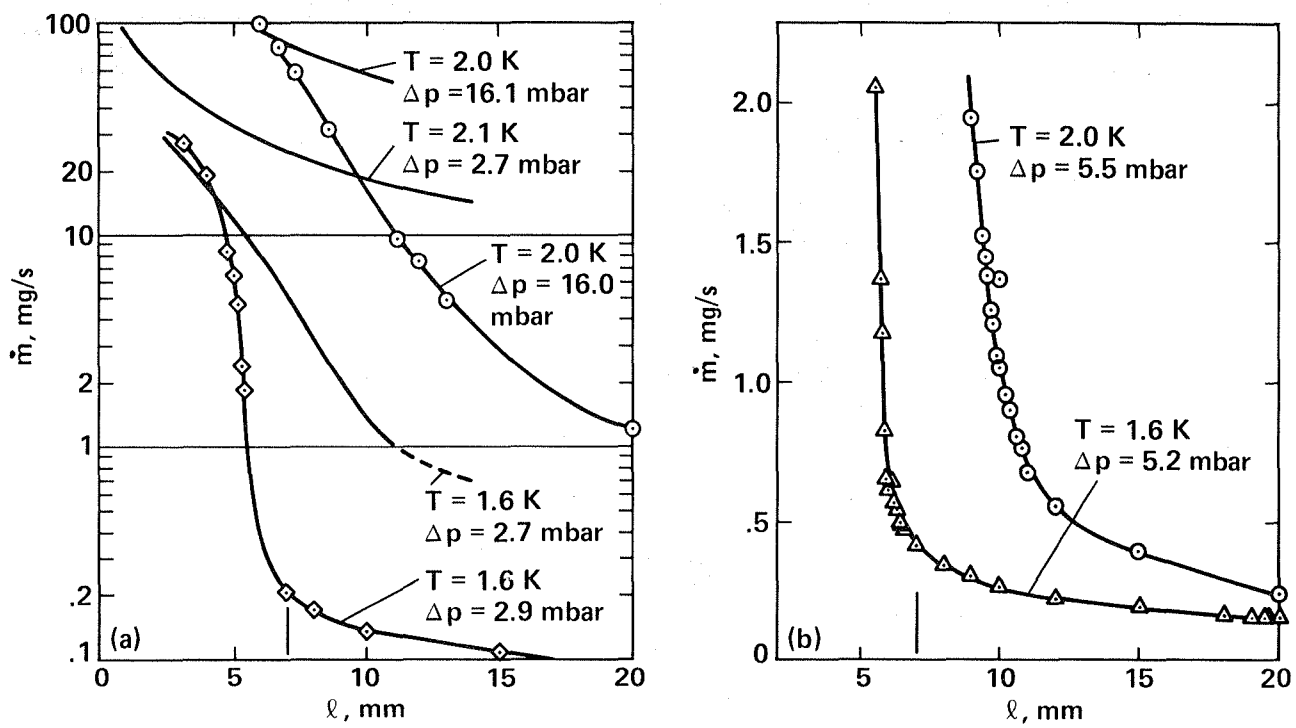

(a) Pin radius R = 10 mm, curves + and o; pin radius R = 5 mm, full lines.

(b) Pin radius R = 10 mm.

Figure 19.- Mass-flow rate vs ℓ for constant T_b and ΔP of the APS (ref. 38).

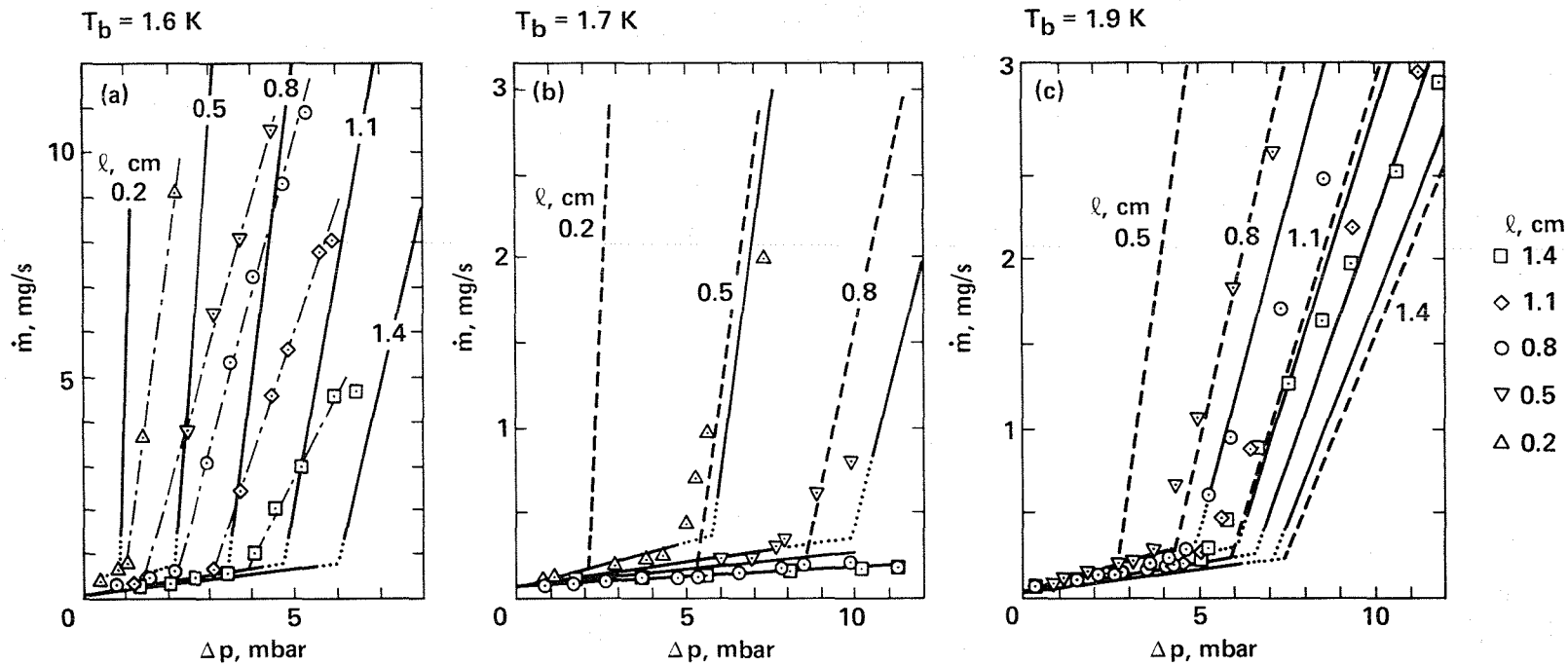

(a) 14-μm gap. (b) 9-μm gap. (c) 9-μm gap.

Figure 20.- Mass-flow rate vs ΔP for various constant ℓ and T_b for the APS (ref. 16). Symbols represent data points, full lines are given by equation (16).

1. Report No.	2. Government Accession No.	3. Recipient's Catalog No.
NASA TM-85966		

4. Title and Subtitle	5. Report Date
SUPERFLUID HELIUM II LIQUID-VAPOR PHASE SEPARATION: TECHNOLOGY ASSESSMENT	July 1984
	6. Performing Organization Code ATP
7. Author(s) Jeffrey M. Lee	8. Performing Organization Report No. A-9768
	10. Work Unit No. T-3491
9. Performing Organization Name and Address Ames Research Center Moffett Field, CA 94035	11. Contract or Grant No.
	13. Type of Report and Period Covered Technical Memorandum
12. Sponsoring Agency Name and Address National Aeronautics and Space Administration Washington DC, 20546	14. Sponsoring Agency Code 423-30-01

15. Supplementary Notes

Point of contact: J. M. Lee, Ames Research Center, MS 244-7, Moffett Field, CA 94035 (415) 965-6533 or FTS 448-6533

16. Abstract

A literature survey of helium-II liquid-vapor phase separation is presented. Currently, two types of He-II phase separators are being investigated: porous, sintered metal plugs and the active phase-separator. The permeability K_p shows consistency in porous-plug geometric characterization. Passive phase-separation using porous plugs has been demonstrated for heat fluxes ranging from 1.0 mW/cm^2 to 100 mW/cm^2, with corresponding mass fluxes of from 0.1 $mg/sec.cm^2$ to 10 $mg/sec.cm^2$, respectively. These results cover a K_p range of 10^{-11} cm^2 to 10^{-9} cm^2. Both the heat and mass fluxes increase with K_p. Downstream pressure regulation to adjust for varying heat loads and bath temperatures is possible. For large dynamic heat loads, the active phase-separator has shown a maximum heat-rejection rate of up to 2 W and bath temperature stability of 0.1 mK. This report recommends that porous-plug phase-separation performance be investigated for application to SIRTF and, in particular, that plugs of 10^{-9} $cm^2 < K_p < 10^{-8}$ cm^2 in conjunction with downstream pressure regulation be studied.

17. Key Words (Suggested by Author(s))	18. Distribution Statement
Helium II, Phase separation, Permeability, Porous plug	Unlimited Subject category: 34

19. Security Classif. (of this report)	20. Security Classif. (of this page)	21. No. of Pages	22. Price*
Unclassified	Unclassified	40	A03

*For sale by the National Technical Information Service, Springfield, Virginia 22161

End of Document